Global Change Biology (2009) **15**, 578–600, doi: 10.1111/j.1365-2486.2008.01679.x

# Assessing the response of area burned to changing climate in western boreal North America using a Multivariate Adaptive Regression Splines (MARS) approach

MICHAEL S. BALSHI*†, A. DAVID McGUIRE‡, PAUL DUFFY§, MIKE FLANNIGAN¶, JOHN WALSH‖ and JERRY MELILLO**

*Department of Biology and Wildlife, University of Alaska Fairbanks, Fairbanks, AK 99775, USA, †Complex Systems Research Center, University of New Hampshire, Durham, NH 03824, USA, ‡US Geological Survey, Alaska Cooperative Fish and Wildlife Research Unit, University of Alaska Fairbanks, Fairbanks, AK 99775, USA, §Neptune & Company, Lakewood, CO 80215, USA, ¶Canadian Forest Service, Great Lakes Forestry Centre, Sault Ste. Marie, ON, Canada P6A 2E5, ‖International Arctic Research Center, University of Alaska Fairbanks, Fairbanks, AK 99775, USA, **The Ecosystems Center, Marine Biological Laboratory, Woods Hole, MA 02543, USA

## Abstract

**Fire is a common disturbance in the North American boreal forest that influences ecosystem structure and function. The temporal and spatial dynamics of fire are likely to be altered as climate continues to change. In this study, we ask the question: how will area burned in boreal North America by wildfire respond to future changes in climate? To evaluate this question, we developed temporally and spatially explicit relationships between air temperature and fuel moisture codes derived from the Canadian Fire Weather Index System to estimate annual area burned at 2.5° (latitude × longitude) resolution using a Multivariate Adaptive Regression Spline (MARS) approach across Alaska and Canada. Burned area was substantially more predictable in the western portion of boreal North America than in eastern Canada. Burned area was also not very predictable in areas of substantial topographic relief and in areas along the transition between boreal forest and tundra. At the scale of Alaska and western Canada, the empirical fire models explain on the order of 82% of the variation in annual area burned for the period 1960–2002. July temperature was the most frequently occurring predictor across all models, but the fuel moisture codes for the months June through August (as a group) entered the models as the most important predictors of annual area burned. To predict changes in the temporal and spatial dynamics of fire under future climate, the empirical fire models used output from the Canadian Climate Center CGCM2 global climate model to predict annual area burned through the year 2100 across Alaska and western Canada. Relative to 1991–2000, the results suggest that average area burned per decade will double by 2041–2050 and will increase on the order of 3.5–5.5 times by the last decade of the 21st century. To improve the ability to better predict wildfire across Alaska and Canada, future research should focus on incorporating additional effects of long-term and successional vegetation changes on area burned to account more fully for interactions among fire, climate, and vegetation dynamics.**

*Keywords:* boreal forest, climate change, fire, future area burned, Multivariate Adaptive Regression Splines

*Received 27 July 2007; revised version received 3 December 2007 and accepted 19 March 2008*

Correspondence: Michael S. Balshi, Complex Systems Research Center, University of New Hampshire, 39 College Road, Durham, NH 03824, USA, tel. + 1 603 862 4434, fax + 1 603 862 0188, e-mail: m.balshi@unh.edu

## Introduction

The North American boreal forest is part of one of the world's most extensive biomes. Wildfire is a common occurrence in this region that affects the structure as

well as functioning of boreal ecosystems. The frequency and size of fires has a close association with climate (Clark, 1990; Flannigan & Van Wagner, 1991; Johnson & Wowchuk, 1993; Skinner *et al*., 1999, 2002; Duffy *et al*., 2005) and future changes in climate are likely to have pronounced effects on fire regime (Wotton & Flannigan, 1993; Flannigan *et al*., 2000, 2005; Carcaillet *et al*., 2001). Changes in the fire regime, defined as frequency, intensity, seasonal timing, type, severity, and size of fire (Weber & Flannigan, 1997), have implications for the climate system through a variety of feedbacks (Kasischke *et al*., 1995). Trace gas emissions due to fire can increase the concentrations of greenhouse gases, creating a positive feedback on climate warming (Gillett *et al*., 2004). Alteration in surface energy exchange as a result of successional dynamics following the fire also alters feedbacks to regional climate (Chapin *et al*., 2000; Chambers & Chapin, 2003; Randerson *et al*., 2006). Given the potential for future climate change in this region, it is important to assess its effect on the future fire regime as it has major implications for carbon cycling (Zhuang *et al*., 2006; Balshi *et al*., 2007), energy feedbacks to the climate system (Randerson *et al*., 2006), and human well being (Chapin *et al*., 2008). In this study, we specifically evaluate how future climate change may affect area burned in boreal North America.

The fire season in the North American boreal forest typically begins in April and continues through September (Skinner *et al*., 2002). Lightning is the primary source of wildfire ignition in boreal North America and usually results in fires that account for the majority of the area burned in a given season (Nash & Johnson, 1996). Smaller fires occur most frequently in the boreal region; however, the majority of the area burned in the boreal forest is the result of large, infrequent fires (Stocks *et al*., 2002) that occur during extended periods of high pressure systems that result in fuel drying (Johnson & Wowchuk, 1993; Macias Fauria & Johnson, 2006). Weather plays a major role in the ignition, growth, and death of a wildfire at daily to monthly time scales (Johnson, 1992; Campbell & Flannigan, 2000; Flannigan *et al*., 2000), and influences fire activity through impacts on fuel moisture, ignitions by lightning, and wildfire behavior. Of these factors, fuel moisture content is one of the most important as it integrates information about temperature and precipitation through time, and hence is a useful indicator of whether or not a fire will start and spread (Flannigan & Harrington, 1988). Fuels for fires may consist of both living vegetation ('live' fuels), detritus on the soil surface, and organic matter in the soil itself ('dead' fuels). Live fuels generally contain significantly more moisture than dead fuels. Prolonged periods of low rainfall and elevated temperatures can lead to a decrease in dead fuel moisture and therefore an increase in the probability of occurrence of a fire event. Factors that contribute to a change in dead fuel moisture include the amount and duration of a precipitation event, temperature, relative humidity, and wind. Each of these factors, in combination with the fuel size and shape, influences the rate at which fuels can retain or lose moisture content.

A variety of studies have been conducted that address how fire weather indices will change under current (Amiro *et al*., 2004) and future climate change scenarios (Flannigan *et al*., 1998, 2000; Stocks *et al*., 1998). Empirical relationships between weather/climate and historical area burned have also been developed for the boreal forest (Harrington *et al*., 1983; Flannigan & Harrington, 1988; Flannigan & Van Wagner, 1991; Skinner *et al*., 1999, 2002; Duffy *et al*., 2005; Flannigan *et al*., 2005; McCoy & Burn, 2005) and for regions in the western United States (Swetnam & Betancourt, 1990; Westerling *et al*., 2006). Empirical studies have also considered teleconnection indices [e.g. the Pacific Decadal Oscillation (PDO), the El Nino Southern Oscillation (ENSO), and the Arctic Oscillation (AO)] that represent different modes of variability in atmospheric circulation, and have been able to explain variability in large fire occurrence in boreal North America at interannual, decadal, and century scales (Duffy *et al*., 2005; Macias Fauria & Johnson, 2006). While these studies have been successful in explaining historical variability in area burned, it is desirable to develop temporally and spatially explicit models of area burned for the North American boreal forest with approaches that can be easily coupled to global climate models (GCMs).

The temporal coverage of historical fire datasets for the North American boreal forest now makes it possible to model relationships between fire weather and area burned across this region. Identification of these relationships can aid in the prediction of future spatial and temporal changes in area burned. The focus of this study is to improve our ability to predict the response of historical wildfire regime to fuel moisture indices and air temperature with the overall goal of predicting future area burned across the North American boreal region. Our first objective is to take an alternative approach to modeling area burned by developing temporally and spatially explicit empirical models using a Multivariate Adaptive Regression Spline (MARS) approach (Friedman, 1991). MARS does not require assumptions to be made about the form of the relationship between the independent and dependent variables. Consequently, it can identify patterns and relationships that are difficult, if not impossible, for other regression methods to reveal. Previous studies have used MARS to model topographic effects on

Antarctic sea ice (De Veaux *et al*., 1993), to map forest characteristics in the western United States (Moisen & Frescino, 2002), and to predict distributions of anadromous fish species in response to various environmental variables (Leathwick *et al*., 2005). A second objective of our study is to use MARS models to generate predictions of annual area burned across boreal North America in response to some scenarios of future climate change.

## Data and methods

### *Overview*

In this study, we evaluated the response of historical wildfires to monthly air temperature and fuel moisture for boreal North America north of 45°N with the goal of developing empirical models that can easily be coupled to GCMs. Thus, our approach was focused on making maximum use of historical data on area burned in Alaska and Canada to develop models with substantial predictive power. We developed temporally and spatially explicit empirical models at 2.5° (latitude × longitude) resolution driven by monthly air temperature, fuel moisture codes, and monthly severity rating (MSR) using a MARS modeling approach to predict annual area burned. Climate predictors were derived from the NCEP Reanalysis I project (Kalnay *et al*., 1996) at 2.5° spatial resolution (see 'Daily weather data and GCM scenarios'). These climate data were also used to calculate spatially and temporally explicit fuel moisture codes using the equations defined in the Canadian Fire Weather Index (CFWI) System (see 'Canadian Fire Weather Index'). We assumed all fires to be the result of lightning ignition as several studies have identified that most of the area burned in boreal North America is associated with lightning-caused fires (Kasischke *et al*., 2002, 2006; Stocks *et al*., 2002; Calef *et al*., 2008). The MARS approach was used to identify relationships between historical annual area burned (1960–2002) and air temperature and fuel moisture at 2.5° spatial resolution. We then evaluated model performance by comparing predictions with observations over the period 1960–2002 across the study region. Model performance was validated against independent data for years 2003–2005 across Alaska and Canada. Following model development, we used climate model output from the second generation of the Canadian Center for Climate Modeling and Analysis Coupled Global Climate Model (CGCM2) to calculate fuel moisture codes for the period 2006–2100 based on the IPCC Third Assessment (IPCC, 2001). We then used the future air temperature and fuel moisture codes to drive each MARS model through year 2100.

### *MARS*

The MARS models use a nonparametric modeling approach that does not require assumptions about the form of the relationship between the predictor and dependent variables (Friedman, 1991). As a consequence, MARS models have the ability to characterize relationships between explanatory and response variables that are difficult, if not impossible, for other regression methods (e.g. linear models) to reveal. In the simplest form, MARS modeling partitions the parameter hyperspace of explanatory variables into disjoint hyperregions. Within each of these hyperregions, a linear relationship is used to characterize the impact of explanatory variables on the response. The point where the slope changes among hyperregions is called a knot and the collection of knots identified by the MARS algorithm is used to generate basis functions (splines), representing either single variable transformations or multivariable interactions.

The MARS algorithm operates in two basic parts. The first part can be thought of as a selection of a suitable collection of explanatory variables, and the second part is the elimination of the least useful explanatory variables among the previously selected set. The first part of the MARS algorithm constructs models in a parsimonious manner by minimizing mean square error (MSE) across the model space while searching in a forward stepwise manner for combinations of variables and knot locations that improve the model fit. Specifically, the basic algorithm cycles through each predictor variable, $x_i$, and every possible knot value, $k$ of $x_i$, and breaks the data into two parts, one on either side of the knot, $k$. The algorithm keeps the knot and variable pair that gives the best fit and then fits the response using linear functions that are both nonzero on one side of the knot. After a variable is selected, splits on subsequent variables can depend on the previous split by splitting on one side of the previous knot (i.e. dependent on the parent basis function).

The number of basis functions can be constrained by a user-defined maximum. The set of explanatory variables is then pruned back (i.e. variables are assessed for potential removal from the model) based on a residual sum of squares criteria using a reverse stepwise procedure. The optimal model is then chosen based on a generalized cross-validation (GCV) measure of the MSE. The GCV procedure is used to determine which variables to keep in a given model by introducing a penalty on adding variables to the model. The procedure determines which variables to keep in the model and which to eliminate. Furthermore, the GCV is used to rank variables in terms of their importance by computing the GCV with and without each variable in the model.

*Model development and extrapolation*

In this study, we used MARS v2.0 (©Salford Systems, 2001, MARS™ v2.0, San Deigo, CA, USA) to develop 127 independent models at 2.5° spatial resolution (total of 127 boreal cells across Alaska and Canada). The total number of models developed depended on the spatial and temporal coverage of historical fire records across the North American boreal region. The parameterization approach was designed to capture variation in the influence of predictor variables across the spatial extent of our domain (e.g. Alaska to Eastern Canada). The response variable is annual area burned and the predictor variables are monthly (April–September) air temperature and the monthly fuel moisture codes and severity rating of the CFWI System (see 'Canadian Fire Weather Index'), for a total of 30 possible predictor variables for each grid cell [6 months × 5 predictors: air temperature, fine fuel moisture code (FFMC), drought code (DC), duff moisture code (DMC), monthly severity rating (MSR)]. Models were only developed for cells where the number of fire years (i.e. years where area burned is nonzero) in a given 2.5° cell is $\geq 10$.

We evaluated the response of annual area burned to future climate change by calculating the CFWI fuel moisture and severity rating components using the CGCM2 GCM A2 and B2 SRES (Special Report on Emission Scenarios) scenario datasets and then extrapolated each MARS model from the year 2006 to the year 2100 for each scenario.

*Datasets for model development and application*

*Historical fire records.* As lightning is caused by weather-related factors, and because our overall goal is to model the influence of fire weather on annual area burned, we do not include human-caused fires in this study. Although human-caused fires account for the majority of fires in the North America boreal region, they account for a small portion of the total area burned (Kasischke *et al*., 2006). For this study, we considered only lightning-caused fires from each dataset for years 1960–2002. The fire data were aggregated by year within each 2.5° grid cell.

A database of fire point location data and 1 km resolution fire-scar datasets was acquired for Alaska and Canada. For Alaska, we used the Alaska fire-scar location database initially developed by Kasischke *et al*. (2002) and maintained by the Bureau of Land Management, Alaska Fire Service (2005). The database contains point and boundary location information for fires in Alaska from 1950 to 2002. Fires >1000 acres (~404 ha) are included from 1950 to 1987, inclusive, and fires >100 acres (~40.4 ha) are included from 1988 to 2002, inclusive. As stated earlier, we used only the data from 1960 to 2002 to develop the empirical models for Alaska.

For Canada, we used a combination of point location data from the Canadian Large Fire Database (LFDB) and provincial polygon data. The LFDB is a compilation of provincial and territorial wildfire data that represents all fires that are >200 ha that occurred from 1959 to 1999. For the point location datasets for Alaska and Canada, we used the longitudinal and latitudinal point locations to calculate a radius for each location based on the area of the historical fire area. Circular fire boundaries were then created for each point by buffering each point by a distance equal to the calculated radius. The provincial polygon data represents fires in all provinces from 1980 to 2002 [Stocks *et al*., 2002; M. D. Flannigan, Canadian Large Fire Database, 1980–2003 (polygon), unpublished data]. Historical fire data for Saskatchewan (Naelapea & Nickeson, 1998) and Alberta (Government of Alberta, 2005) were also obtained as polygon coverages for the periods 1945–1979 and 1931–1979, respectively. We restricted model development to using historical fire data from 1960 to 2002 and prioritized the use of burned area from polygon data over point location.

*Daily weather data and GCM scenarios.* Daily maximum air temperature, wind speed, and relative humidity were obtained from the NCEP Reanalysis 1 dataset (Kalnay *et al*., 1996) at the NOAA/OAR/ESRL PSD, Boulder, CO, USA (http://www.cdc.noaa.gov/) at 2.5° resolution for the years 1960–2005. For daily precipitation, we used the statistically reconstructed NCEP precipitation obtained online from the Arctic RIMs data server (http://rims.unh.edu/data/data.cgi) at 2.5° resolution for the period 1960–2005. The daily NCEP data were used to calculate the fuel moisture components of the CFWI System (refer to 'Canadian Fire Weather Index'). The fuel moisture codes and air temperature were then aggregated to monthly resolution to develop empirical relationships with historical area burned using the MARS modeling approach (refer to 'Datasets for model development and application').

To predict annual area burned for future scenarios of climate change, we derived daily data from 1961 to 2100 at approximately 3.75° × 3.75° resolution for air temperature, precipitation, specific humidity, and wind speed from the second generation of CGCM2 (http://www.cccma.bc.ec.gc.ca/data/cgcm2/cgcm2.shtml). A detailed description of the CGCM2 can be found in Flato & Boer (2000). CGCM2 has been used to produce ensemble climate change projections using the IPCC Third Assessment A2 and B2 scenario storylines. The A2 and B2

 

emissions storylines are discussed in detail in the IPCC Special Report on Emissions Scenarios (Nakićenović & Swart, 2000). The emissions scenarios act as representations of the future development of radiatively active emissions and are based on assumptions about socioeconomic, demographic, and technological changes. These scenarios are then converted into greenhouse gas concentration equivalents that are used as driving variables for GCM projections. The A2 scenario represents a world where energy usage is high, economic and technological development is slow, and population growth reaches 15 billion by the year 2100. The B2 scenario represents a world where energy usage is lower, economies evolve more rapidly, environmental protection is greater, and population growth is slower (10.4 billion by the year 2100). The B2 scenario therefore produces lower emissions and less future warming.

Both scenarios have a baseline period of 1961–1990 that corresponds to the IS92a scenario which is used to initialize the A2 and B2 scenarios for CGCM2. These data were downscaled from 3.75° to 2.5° spatial resolution by area-weighting the CGCM2 cells that intersected a given 2.5° grid cell. To account for differences between the model development data and the GCM predictions (air temperature, relative humidity, precipitation, and wind speed), we adjusted the CGCM2 data relative to the absolute difference from the 1961–1990 NCEP mean by

$$\mathrm{CGCM2}_{\mathrm{adjusted\,daily}} = \mathrm{NCEP}\mu + \left(\mathrm{CGCM2}_{\mathrm{daily}} - \mathrm{CGCM2}\mu\right), \quad (1)$$

in which NCEP$\mu$ is the mean daily value (across all years) for the period 1961–1990 derived from the NCEP model development data, $\mathrm{CGCM2}_{\mathrm{daily}}$ is the daily value output by CGCM2, and CGCM$\mu$ is the mean daily value (across all years) for the period 1961–1990 derived from the CGCM2 daily data. Taking the absolute difference between different climate datasets can result in unrealistic values, particularly for precipitation (e.g. negative values for precipitation). Only five precipitation data points [calculated by Eqn (1)] across the study area resulted in negative values, and we set these points to zero.

*Canadian Fire Weather Index.* The CFWI was developed for the prediction of forest fire behavior in response to weather data (Van Wagner, 1987). The CFWI is composed of three fuel moisture codes: DC, DMC, and the FFMC, and three behavioral indices which are the buildup index (BUI), initial spread index (ISI), and fire weather index (FWI). Of the three behavioral indices, the FWI represents the intensity of a spreading fire and is derived from the three moisture codes and surface wind speed. The daily severity rating (DSR) is derived from the FWI and is designed to capture the nonlinear aspect of fire spread (area burned) (Van Wagner, 1987). By averaging the DSR over a period, one can obtain the MSR or seasonal severity rating (SSR), which are used as indices of fire weather from month to month (MSR) and from season to season (SSR). Each component of the CFWI system is calculated from a combination of daily weather data that include air temperature, precipitation, relative humidity, and wind speed. It should be noted that many of the components of the CFWI System are highly nonlinear.

For the purpose of this study, we use the fuel moisture codes and severity rating. The unitless codes represent the amount of moisture present in organic matter, with higher values indicative of less moisture content in fuels. The FFMC represents the moisture content of surface litter and other fine fuels in a forest stand and is an indicator of sustained flaming ignition and fire spread. The DMC represents the moisture content of loosely compacted, decomposing organic matter of moderate depth and relates to the probability of lightning ignition and fuel consumption. The DC represents a deep layer of compact organic matter and relates to the consumption of heavier fuels and the effort required to extinguish a fire.

We used the CFWI algorithm (provided by Mike Wotton, personal communication) to calculate 2.5° estimates of the fuel moisture and DSR codes for each day for the months April to September (years 1960–2005) across Alaska and Canada. For the period 1960–2005, we used the daily air temperature, precipitation, relative humidity, and wind speed values from the NCEP Reanalysis I dataset to calculate the fuel moisture codes and DSR that were then aggregated to monthly resolution for model input. For evaluating fire regime for future scenarios of climate change, a second set of spatially explicit CFWI fuel moisture and severity codes was calculated for years 2006–2100 based on the CGCM2 A2 and B2 scenarios.

## Results

We first present our model estimates that correspond to the temporal period of the development datasets (1960–2005) and discuss model performance at different spatial scales. We then present estimates of annual area burned for future scenarios of climate change.

### *Model estimates for Alaska and Canada, 1960–2005*

At 2.5° resolution, our models captured the variation in annual area burned across Alaska and Canada with

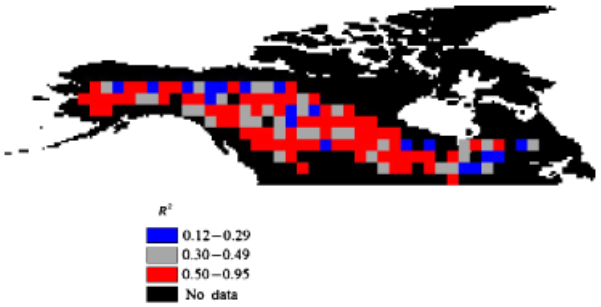


**Fig. 1** $R^2$ values for each 2.5° model developed for Alaska and Canada to predict area burned based on observed area burned from 1960 to 2002.

**Table 1** (a) Model variables and the number of times they occurred across all 2.5° models ($N = 127$) for Alaska and Canada and (b) the number of times a variable entered the model as the most important predictor

| Model variable | April | May | June | July | August | September |
|---|---|---|---|---|---|---|
| (a) Variable count | | | | | | |
| Air temperature | 22 | 10 | 18 | 33 | 22 | 8 |
| MSR | 20 | 12 | 21 | 17 | 12 | 8 |
| DC | 6 | 10 | 6 | 23 | 16 | 6 |
| DMC | 3 | 6 | 18 | 11 | 1 | 3 |
| FFMC | 5 | 4 | 7 | 3 | 6 | 6 |
| (b) Variable importance | | | | | | |
| Air temperature | 6 | 2 | 8 | 16 | 11 | 2 |
| MSR | 8 | 2 | 5 | 8 | 7 | 3 |
| DC | 3 | 5 | 1 | 8 | 10 | 0 |
| DMC | 1 | 1 | 8 | 3 | 0 | 1 |
| FFMC | 1 | 1 | 3 | 0 | 2 | 1 |
| Sum of CFWI codes | 13 | 9 | 17 | 19 | 19 | 5 |

MSR, monthly severity rating; DC, drought code; DMC, duff moisture code; FFMC, fine fuel moisture code; and CFWI, Canadian Fire Weather Index.

**Table 2** Observed and predicted annual area burned for Alaska and Canada* for years 2003–2005

| Region | Year | Observed area burned ($km^2$) | Predicted area burned ($km^2$) |
|---|---|---|---|
| Canada | 2003 | 23 764 | 11 969 |
| | 2004 | 33 615 | 32 222 |
| | 2005 | 13 183 | 14 376 |
| Alaska | 2003 | 2350 | 3511 |
| | 2004 | 26 326 | 6377 |
| | 2005 | 18 602 | 4594 |

Observations for Alaska were derived from an updated version of the Alaska fire-scar database. Estimates for Canada are satellite-derived and were produced by Fraser *et al*. (2000). Predicted area burned was obtained by driving the MARS (Multivariate Adaptive Regression Splines) fire models with CFWI (Canadian Fire Weather Index) codes based on NCEP climate data for the years 2003–2005.

*The reporting of predicted area burned for Canada is for western Canada only, while the reporting of observed area burned is for all of Canada for which most of the area burned in 2003, 2004, and 2005 occurred in western Canada.

varying levels of success (Fig. 1). On average, the models explained 53% of the variation in annual area burned at 2.5° resolution. Across all models (see Appendix A), monthly air temperature was found to be the most frequently occurring variable followed by MSR (Table 1a). Across all variables, the months June through August were the most frequently occurring months across all models (Table 1). The starting (April and May) and ending (September) months for all variables generally had the fewest occurrences across all models. On an individual basis, July air temperature entered the models most frequently as the variable of greatest importance (Table 1b). However, if the CFWI codes are grouped together, they enter the models most frequently for months June through August as the most important predictors of area burned, followed by July temperature (Table 1b).

To maximize the predictive ability of the models developed in this study, we made extensive use of the fire-scar data for Alaska and Canada from 1960 to 2002. Independent data for Alaska (Bureau of Land Management, Alaska Fire Service, 2005) and Canada (based on Fraser *et al*., 2000) now exist for years 2003–2005 that can be compared with the estimates produced in our study (Table 2). For Canada, the estimates of annual area burned are within approximately 1400 $km^2$ of the observed area burned in 2004 and 2005, but area burned is underestimated by approximately 11 000 $km^2$ in 2003. For Alaska, the models overestimate annual area burned by approximately 1200 $km^2$ in 2003, but substantially underestimate area burned in the years 2004 and 2005 (Table 2). However, the models do identify 2004 in Alaska as having approximately 40% more area burned than 2005, which is consistent with the observations of relative areas actually burned in those years.

Differences in the level of predictability at 2.5° are related to the region in which a given model was developed (Figs 1 and 2). The models appear to consistently capture the variability in annual area burned in the western portion of the study area, extending from the interior region of Alaska through portions of western and central Canada. The models have weak predictive capability (i.e. lower explanatory power) in areas along the boreal forest–tundra border in western

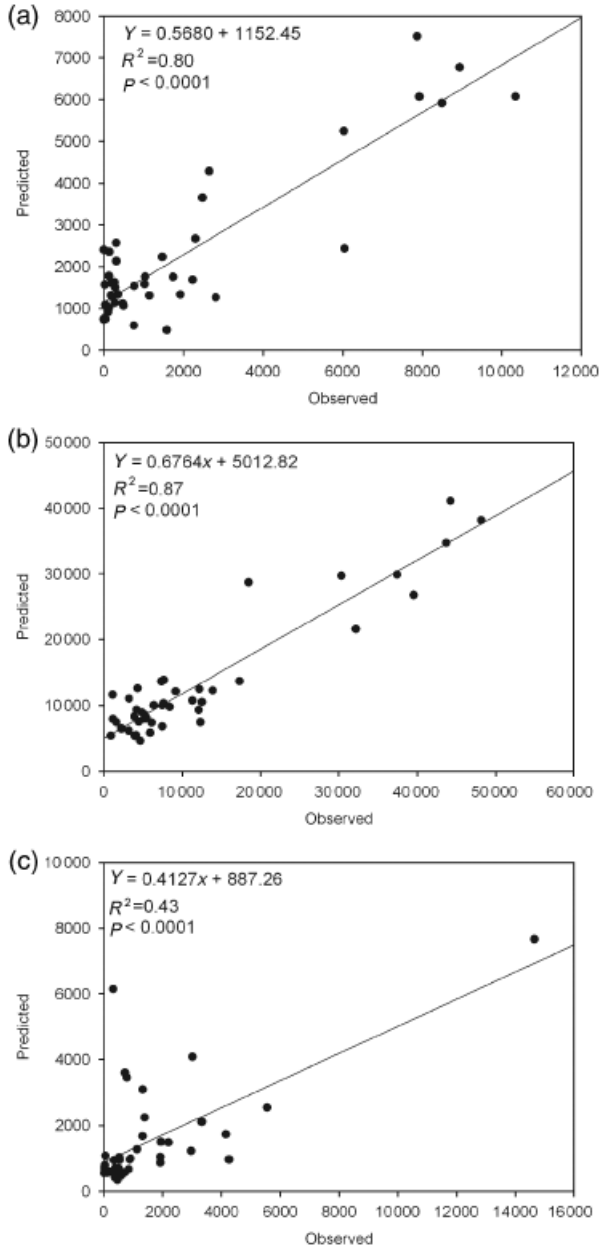


**Fig. 2** Observations vs. MARS (Multivariate Adaptive Regression Splines) model predictions ($km^2$) from 1960 to 2002 aggregated to regional scales for Alaska (17 models aggregated) (a), western Canada (91 models aggregated) (b), and eastern Canada (19 models aggregated) (c).

boreal North America, as well as throughout eastern boreal North America extending from southeast of the Canadian Shield through Ontario and Quebec. Areas with substantial topographic relief, such as the MacKenzie mountains and eastern edges of the Rocky Mountains also have lower levels of predictability. To give a better picture of the level of predictability aggregated to the regional scale, we divided the study area into three regions: Alaska (defined as west of 145°W), western Canada (defined as east of 142.5°W and west of 92.5°W, extending southeast from the Yukon Territory to eastern Manitoba), and eastern Canada (defined as east of 90°W) extending from western Ontario to western Newfoundland). For Alaska ($N_{models} = 17$; Fig. 2a) and western Canada ($N_{models} = 91$; Fig. 2b), the MARS approach explains on the order of 80% of the variation in annual area burned, with greater predictability in western Canada. In general, the models in Alaska (Fig. 2a) and western Canada (Fig. 2b) tend to underestimate area burned in large fire years, with the bias being more substantial in Alaska, and tend to overestimate area burned in small fire years. In contrast to Alaska and western Canada, the models for eastern Canada ($N_{models} = 19$; Fig. 2c) explain only about 40% of the variation in annual area burned, and most of this variation explained is driven by an outlying data point from an anomalously large fire year. Removing this data point caused the models to collectively explain only 9% of the variation in annual area burned for eastern Canada.

Because of the low level of predictability for eastern Canada, we excluded this region from further analyses and applications of predicting area burned under future scenarios of climate change. To analyze the level of predictability at the scale of Alaska and western Canada combined, we aggregated the predicted annual area burned for the period 1960–2002 and compared it with observations contained in all model cells over that period. At this scale (Alaska and western Canada combined), the MARS models explain 82% ($P < 0.0001$) of the variation in annual area burned in response to April–September air temperature, FFMC, DMC, DC, and MSR (Fig. 3a). The models capture the interannual variation in observed annual area burned, from small fire years to large fire years (Fig. 3b), as well as the trend of increasing area burned from 1960 to 2002. However, the trend in predicted annual area burned ($226\,km^2\,yr^{-1}$; $R^2 = 0.09$; $P < 0.05$) is approximately half of that of the trend in observed area burned ($459\,km^2\,yr^{-1}$; $R^2 = 0.19$; $P < 0.05$). The models tend to overestimate annual area burned on average by approximately 50% during the early- to mid-1960s and underestimate area burned during large fire years from the late 1970s through 2002. Observed area burned tends to be small before the late 1970s, and the five large fire years in the record (years with more than $20\,000\,km^2$ burned) occurred after the late 1970s. Therefore, the biases in estimating area burned before and after the late 1970s appears to be associated with the tendency of the models to overestimate area burned in small fire years and underestimate area burned in large fire years (Fig. 2a and b).

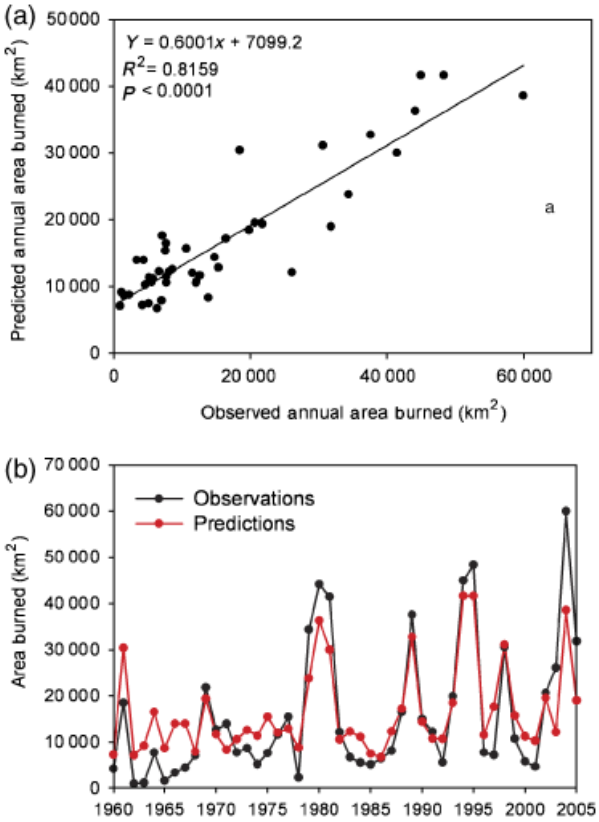


**Fig. 3** (a) Observed vs. predicted annual area burned for Alaska and western Canada for years 1960–2002. (b) Comparison of observed and predicted area burned for years 1960–2005.

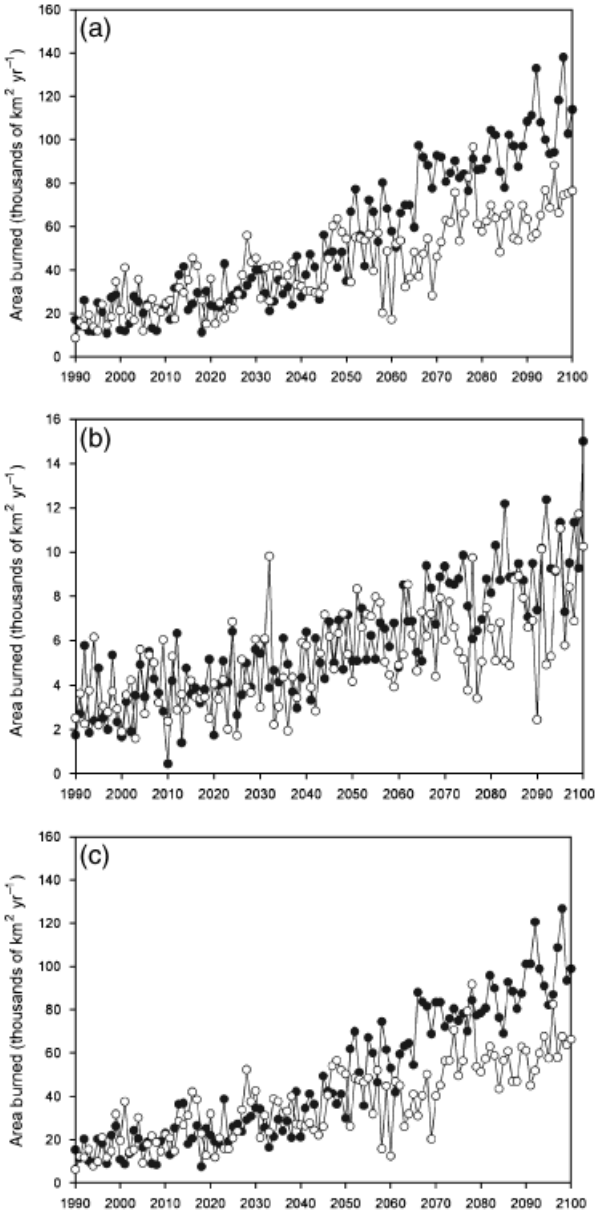


**Fig. 4** Predicted annual area burned (thousands of $km^2 yr^{-1}$) driven by using the NCEP model development datasets ('Observed'; 1990–2005) and the CGCM2 A2 and B2 Scenarios (2006–2100) for Alaska and western Canada (a), Alaska (b), and western Canada (c). Dark circles represent the estimates driven by the A2 scenario while the open circles represent the estimate driven by the B2 scenario. Note that the scale for Alaska (b) is a factor of 10 lower than the parts (a) and (c).

### *Future area burned, 2006–2100*

At the scale of Alaska and western Canada, future area burned shows substantial interannual variability from year to year when forced by the A2 and B2 climate scenarios (Fig. 4a). Predicted area burned between the A2 and B2 scenarios is similar through 2050, but diverges for the last 50 years of the 21st century, with the A2 scenario resulting in greater area burned (Fig. 4a). We averaged area burned by decade from 1991 to 2100 to highlight the differences between each scenario. The period 1991–2000 is defined as the baseline comparison period. This corresponds to a period with high fire activity across Alaska and western Canada and is used to compare with future decades that are also assumed to experience high levels of fire activity in response to climate change. Across Alaska and western Canada, average area burned approximately doubles by the middle of the 21st century for both the A2 and B2 scenarios. Under the A2 scenario, area burned continues to increase on the order of 1.2 × per decade from 2050 to 2100 (Fig. 5a). Relative to 1991–2000, area burned increases by 5.5 × under the A2 scenario by the last decade of the 21st century. A period exists under the B2 scenario where average area burned plateaus from the 2040s until the 2060s followed by an increase in the 2070s that remains approximately the same through the remaining decades of the 21st century

 

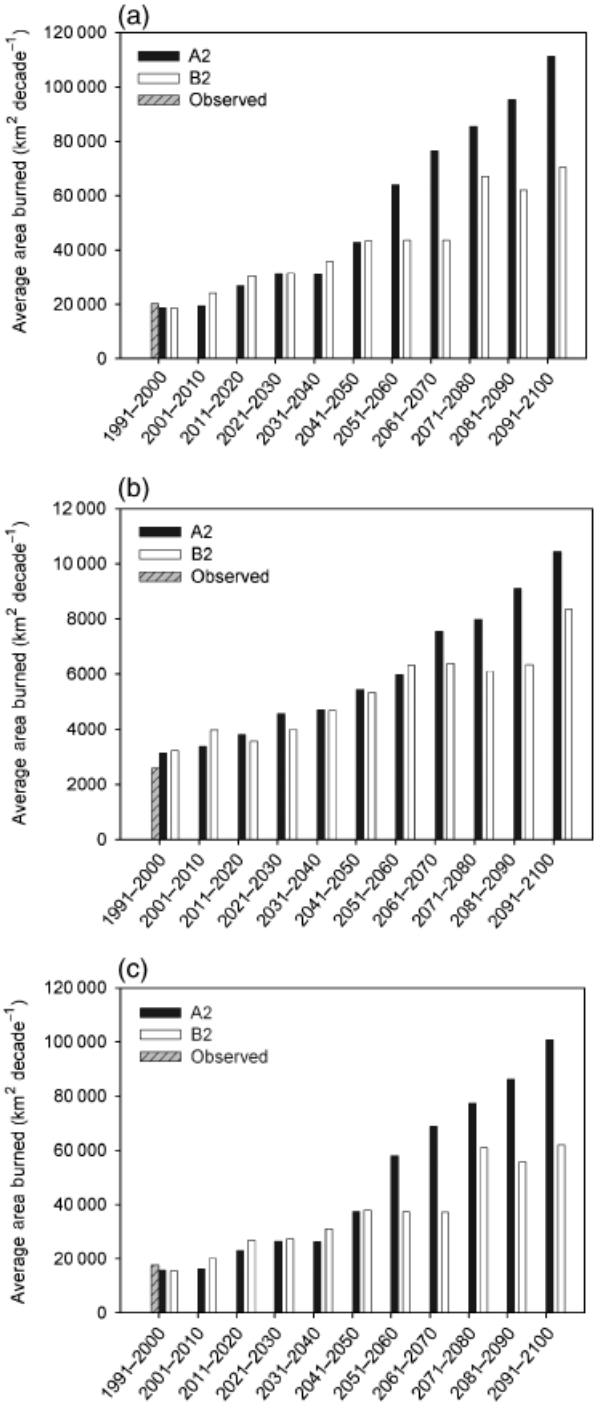


**Fig. 5** Predicted mean annual area burned (km$^2$ yr$^{-1}$) per decade for Alaska and western Canada (a), Alaska (b), and western Canada (c) driven by the NCEP model development datasets (1990–2005) and the CGCM2 A2 and B2 climate scenarios (2006–2100). The observed baseline decade from 1991 to 2000 was used for comparison with subsequent decades.

(Fig. 5a). Relative to the baseline period, average area burned increases on the order of 3.5 × under the B2 scenario.

To understand the differences in future area burned when moving from Alaska to western Canada, we divided the study area into regions as defined earlier (excluding eastern Canada). Across Alaska (Fig. 4b) and western Canada (Fig. 4c) annual area burned shows considerable variation from year to year under the A2 and B2 scenarios. Relative to the baseline period, average area burned per decade approximately doubles by the 2040s for both Alaska (Fig. 5b) and western Canada (Fig. 5c) under both scenarios. For both subregions, the A2 scenario generally results in an increase in average area burned per decade from the baseline period through the 2090s. Comparing the baseline period with the last decade of the 21st century, the A2 scenario results in an increase in average area burned per decade by 4 × and 5.7 × for Alaska (Fig. 5b) and western Canada (Fig. 5c), respectively. For the B2 scenario, however, area burned appears to plateau from 2050 to 2090 in Alaska (Fig. 5b) and from 2040 to 2070 in western Canada (Fig. 5c). For Alaska, this is followed by an increase in average area burned per decade for the period 2091–2100, while for western Canada an increase in average area burned per decade is observed in 2071–2080 and then remains similar through the end of the 21st century. Relative to the baseline period, average area burned per decade for the 2090s increases on the order of 3.2–3.5 times for both subregions.

## Discussion

The results presented here represent a first attempt at using a nonparametric regression spline approach for understanding the response of historical wildfire regime to fuel moisture indices and weather with the overall goal of predicting future area burned. Below we discuss the overall performance of the MARS modeling approach, the effectiveness of this approach at different spatial and temporal scales, and identify uncertainties and limitations of this approach.

### *Model fitting and overall performance*

While several methods have been successful at regional levels, they are often based on classical linear regression approaches when, in fact, the underlying relationships between climate and fire are inherently nonlinear (Stocks, 1993). The use of classical regression techniques such as simple or multiple linear regression for describing complex relationships is limited as the models may be too simplistic to accurately represent the study system. Additionally, these methods tend to be cumbersome in terms of meeting assumptions of data normality, often require variable transformations, and are not efficient for investigating relationships hidden in data-

sets of high dimensionality. Improvements in identifying complex relationships can be made through the use of more complicated modeling approaches, such as neural networks, but it is often difficult to interpret the meaning of the outputs. The MARS approach is a means of overcoming these hurdles when modeling complex systems by forming a series of regressions on different intervals (hyperregions) of the independent variable space without having to meet the assumptions of data normality. An additional concern when modeling observational data is the problem of extreme collinearity of predictor variables (Friedman, 1991). The effects of having variables that are highly correlated are reduced in the MARS approach by introducing a penalty on added variables through the GCV criterion used in the forward selection procedure, as well as by increasing the number of interaction terms in the model. Furthermore, models developed using the MARS approach are generally easier to interpret in comparison with other modeling and mathematical techniques (e.g. neural networks, principal components analysis). Other empirical approaches have achieved similar or greater levels of predictability of area burned in boreal North America through the use of teleconnection indices that represent temporal and spatial modes of variability in atmospheric circulation (notably Duffy *et al*., 2005; Macias Fauria & Johnson, 2006). While these approaches have been very useful in understanding how atmospheric circulation patterns affect fire regime, we believe that the MARS approach generally takes those effects into account and is more amenable for coupling with GCMs that vary substantially in their ability to represent different temporal modes of variability in atmospheric circulation.

### *Spatial and temporal dynamics of historical wildfire regime*

It is clear that a linkage exists between fire and climate; however, the strength of empirical relationships between historical area burned and the independent variables we considered in this study (specifically the components of the CFWI and air temperature) can vary from one geographic region to another. Understanding the spatial and temporal dynamics of historical area burned is essential before predicting area burned for future scenarios of climate change. Our results are a first attempt at understanding wildfire regime through the use of the MARS modeling approach. We found considerable spatial variation in the level of predictability (i.e. some models explain more variability in annual area burned than others) at 2.5° but were able to explain on the order of 82% of the variation in annual area burned at the scale of Alaska and western Canada. Fire weather indices have been used to establish relationships with area burned by wildfire across Canada in previous studies. For example, Harrington *et al*. (1983) explained up to 38% of the variability in provincial area burned while Flannigan *et al*. (2005) explained between 36% and 64% of the variation in area burned by ecozone (biogeographic region). Both these studies used forward-stepwise linear regression approaches.

Accounting for the spatial influences on wildfire regime is important when developing models that are driven by fuel moisture and temperature. For example, the fire regime across Alaska and western Canada has more continental influences than in eastern Canada, where fire regime is influenced by Atlantic moisture sources and large water bodies (e.g. Great Lakes, Hudson and James Bays). As a result, short-lived drought periods will have a greater influence on fire regime in regions characterized by drier climates while regions characterized by a wetter climate require longer drought periods to realize similar effects (Skinner *et al*., 1999). The fire return interval, defined as the time it takes to burn an area equal in size to an existing burn area, can also influence model development and overall performance. In eastern Canada, the fire return interval tends to be longer (Campbell & Flannigan, 2000) and it may therefore take a longer record of fire in eastern Canada to better quantify the relationship between fire and climate in the context of other factors that may influence the fire regime, (e.g. more extensive low flammability broad leaf forests). However, it is notable that the AO is able to explain 68% of area burned by large fires in eastern Canada after 1976 (Macias Fauria & Johnson, 2006).

The level of predictability was generally higher in the western portion of our study area, with some areas of low predictability near the MacKenzie mountain range and along the eastern border of the Rocky Mountains. Low predictability also occurred in areas along the boreal forest–tundra border in western North America. Although we did not incorporate topographic influences on fire regime in this study, it has been shown to be an important factor in previous studies at regional scales (Dissing & Verbyla, 2003). In the eastern portion of the study region, the level of predictability was considerably lower, as also observed in previous studies (Harrington *et al*., 1983; Flannigan & Van Wagner, 1991) and may be attributed to factors such as maritime influences and more extensive use of fire suppression.

Accounting for the seasonality of wildfire regime is an important component of attempts to model the variation in annual area burned. Generally, the mid-summer (June and July) months will correspond to periods of high fire activity in the North American boreal region as they are, on average, the warmest

months and support favorable conditions for fire ignition and spread. Our models demonstrate the ability to capture this period, as the most frequent months that entered a given model across our study area were either June or July. Stocks *et al*. (1998) used the Canadian GCM under a $2\times$ $CO_2$ scenario and found that areas experiencing extreme fire weather danger across Canada and Russia occurred primarily in June and July. It has been observed, however, that in extreme fire years, favorable conditions for fire ignition and spread can occur well beyond this period (for example, 2004 fire season in Alaska). Air temperature has been demonstrated in previous empirical studies to be an important predictor of area burned by wildfire (see Flannigan *et al*., 2001, 2005; Duffy *et al*., 2005). Duffy *et al*. (2005) explained 79% of the variation in annual area burned for Alaska using monthly air temperature, precipitation, and atmospheric teleconnection indices. Our results support the role of air temperature as a predictor of area burned as it entered the models as one of the most important predictors (Table 1b). Macias Fauria & Johnson (2006) also used a spatially explicit modeling approach that employed teleconnection indices to predict area burned across Alaska and Canada and found that the PDO/ENSO patterns successfully explained $>80\%$ of the variability in area burned by large fire events after 1976 in the western half of boreal North America, but only explained about 7% of the area burned before 1976. In contrast to the results of Macias Fauria & Johnson (2006), our models explain considerable variation in annual area burned both before and after the PDO shift that occurred in the mid-1970s. For Alaska and western Canada, our models explain on the order of 42% ($P<0.001$) and 86% ($P<0.00001$) of the variation in annual area burned for the periods 1960–1976 and 1977–2005, respectively. Other studies have found that the fuel moisture codes of the CFWI (FFMC, DMC, DC), were the most frequently occurring predictors of area burned for Canadian ecozones (Flannigan *et al*., 2005). The FFMC, DMC, and DC (in increasing order of importance) were also found to be important in the prediction of area burned in our study; however, air temperature and MSR were the most frequently occurring predictors in the models across Alaska and Canada (Table 1a). With respect to predictor importance, however, the CFWI codes, as a group, entered the models more frequently across the study area (Table 1b).

### *Future wildfire regimes*

The projected changes in climate across the boreal region are expected to have far-reaching effects on fire regime. Shifts in fire size, frequency, and severity would have major implications for the carbon cycle (Zhuang *et al*., 2006; Balshi *et al*., 2007) across this region, as well as energy feedbacks to the climate system (Randerson *et al*., 2006) and potential impacts on regional socioeconomic conditions (Chapin *et al*., 2003). Various forcing scenarios that drive GCMs make it possible to understand how fire regime might change by the end of the 21st century. In this study, we were limited to using the daily output variables from one GCM as other datasets that were publicly available were not temporally continuous (i.e. they were only represented as time slices for different periods of the 21st century). However, the CGCM ranks among the top GCMs currently used by the IPCC with respect to the level of predictability in northern high latitudes (Table 3).

Future area burned across Alaska and western Canada predicted for the period 2006–2050 indicates marginal differences between the A2 and B2 forcing scenarios (Fig. 4a). Although an increase in average area burned is predicted for the entire study region over this period, the increase in the frequency of the largest fire events is not evident until the late 2040s. Across Alaska and western Canada, annual area burned under the A2 and B2 scenarios are similar through 2050, but diverge in the last 50 years of the 21st century with the climate under the A2 scenario resulting in greater area burned in both regions.

The projected increase in annual area burned across Alaska and western Canada is similar to those estimates presented in previous studies. Flannigan *et al*. (2005) suggest that under a $3\times$ $CO_2$ scenario, area burned will increase by 74–118% by the end of the 21st century. An earlier study by Flannigan & Van Wagner (1991) explored relationships between SSR and annual provincial area burned. They found that under a $2\times$ $CO_2$ scenario climate, SSR increased by 46% and suggested that an increase in area burned could be expected under similar conditions, but assumed that the relationship between area burned and SSR is linear.

Flannigan *et al*. (2000) investigated the influence of future climate on SSR for forests across the United States. They suggest that under a $2\times$ $CO_2$ climate scenario, SSR will increase by approximately 30% in parts of Alaska, which translates into an increase in area burned between 25% and 50% by the middle of the 21st century. Relative to the period 1991–2000, we predict an approximate doubling of average area burned per decade for Alaska by the 2040s under both the A2 and B2 climate scenarios. Large future increases in area burned for western and central Canada under future climate change scenarios have been suggested by Flannigan *et al*. (2001) due to increases in the FWI. McCoy & Burn (2005) suggest an approximate doubling of area burned for central Yukon Territory by 2069. Tymstra *et al*. (2007) estimate an increase in area burned between 12.9% and

**Table 3** The IPCC climate model ranks based on root mean square errors (RMS) averaged over latitudinal ranges 60–90°N and 20–90°N for surface air temperature (*T*), precipitation (PREC), and sea level pressure (SLP)

| | | 60–90°N | | | 20–90°N | | | |
|---|---|---|---|---|---|---|---|---|
| Rank | Model | T | PREC | SLP | T | PREC | SLP | Total |
| 1 | MPI ECHAM5 (Germany) | 1 | 1 | 3 | 1 | 1 | 1 | 8 |
| 2 | GFDL CM2.1 (USA) | 3 | 4 | 1 | 5 | 2 | 2 | 17 |
| 3 | MIROC3.2_MEDRES (Japan) | 4 | 3 | 6 | 3 | 5 | 8 | 29 |
| *4* | *CCCMA CGCM3.1 (Canada)* | *11* | *2* | *8* | *10* | *4* | *2* | *37* |
| 5 | UKMO HADCM3 (UK) | 8 | 6 | 2 | 6 | 7 | 9 | 38 |
| 6 | MRI CGM2.3.2A (Japan) | 13 | 11 | 5 | 7 | 6 | 4 | 46 |
| 7 | NCAR CCSM3.0 (USA) | 2 | 15 | 8 | 2 | 13 | 7 | 47 |
| 8 | GFDL CM2.0 (USA) | 9 | 8 | 10 | 14 | 4 | 6 | 51 |
| 9 | INMCM3.0 (Russia) | 6 | 7 | 13 | 10 | 9 | 12 | 57 |
| 10 | CNRM CM3 (France) | 5 | 12 | 12 | 5 | 11 | 13 | 58 |
| 11 | NCAR PCM1 (USA) | 13 | 5 | 5 | 14 | 12 | 10 | 59 |
| 12 | CSIRO MK3.0 (Australia) | 14 | 9 | 11 | 12 | 9 | 5 | 60 |
| 13 | IPSL CM4 (France) | 7 | 11 | 9 | 12 | 15 | 11 | 65 |
| 14 | GISS MODEL ER (USA) | 10 | 14 | 14 | 10 | 14 | 15 | 77 |
| 15 | IAP FGOALS1.0.G (China) | 15 | 13 | 15 | 15 | 10 | 14 | 82 |

In all cases, the RMS errors were summed over the seasonal cycle (12 calendar months) to obtain the ranks. The last column in the table is the sum of the ranks in the preceding columns. CGCM is italicized.

29.4% for Alberta under $2\times$ and $3\times$ $CO_2$ climate scenarios. Bergeron *et al*. (2006) suggest an increase in fire frequency in black spruce forests across western Canada while a lower fire frequency in hardwood forests under a $2\times$ and $3\times$ $CO_2$ climate. We estimate that the western Canada subregion (which also encompasses central Canada) will be responsible for the majority of future area burned across North America. By the mid–21st century, we estimate that average area burned per decade will double under the CGCM2 A2 and B2 scenarios and increase by a factor of 3.6–5.6 times by 2091–2100 (Fig. 5c). Historically, this region has been responsible for the majority of area burned across boreal North America.

To assess the reasonableness of our fire model predictions across Alaska and western Canada and how they change through time, we calculated the fire return interval (FRI) based on the methods defined by Balshi *et al*. (2007) for the last 30 years of the historical fire record (Fig. 6a) and the last 30 years of the A2 (Fig. 6b) and B2 (Fig. 6c) climate change scenarios. Predicted area burned under the A2 scenario suggests that average FRIs decrease (i.e. fire activity increases) on the order of 50% in Alaska and 40% in western Canada relative to the historical FRIs in these subregions (Fig. 6b). Relative to the historical FRIs, predicted area burned under the B2 scenario suggest that FRIs decrease on the order of 45% in Alaska and 35% in western Canada (Fig. 6c). Thus, by the end of the 21st century, our predictions suggest that fire activity nearly doubles for the Alaska-western Canada region, with slightly lower fire activity under the B2 climate scenario. These predicted changes in fire cycles of Alaska and western Canada would result in fire cycles that are currently experienced in eastern Siberia (McGuire *et al*., 2002, 2007; Balshi *et al*., 2007).

### *Limitations and uncertainties*

Several factors introduce uncertainty in our ability to predict area burned, including the assumptions underlying the use of the CFWI to estimate fuel moisture and severity components for different forest types, the quality and resolution of future climate datasets, and variables not considered in the present analysis.

The present study assumes that the CFWI, which is based on relationships developed with jack pine and Douglas fir (Van Wagner, 1970), can be applied to other forest types that may have different fuel moisture characteristics. However, seasonal trends in duff moisture dynamics in black spruce feather moss stands were predicted well by the CFWI fuel moisture codes (Wilmore, 2001), suggesting that the CFWI may be robust for conifer forests across boreal North America.

Despite the many shortcomings of GCMs, they are the only available tools for estimating future changes in climate. The coarse spatial resolution of GCM output often requires downscaling to an appropriate resolution for conducting analyses relevant to the objectives of a study. The availability of daily GCM output also restricted our options to the use of only one GCM. Many GCMs provide outputs only for certain time

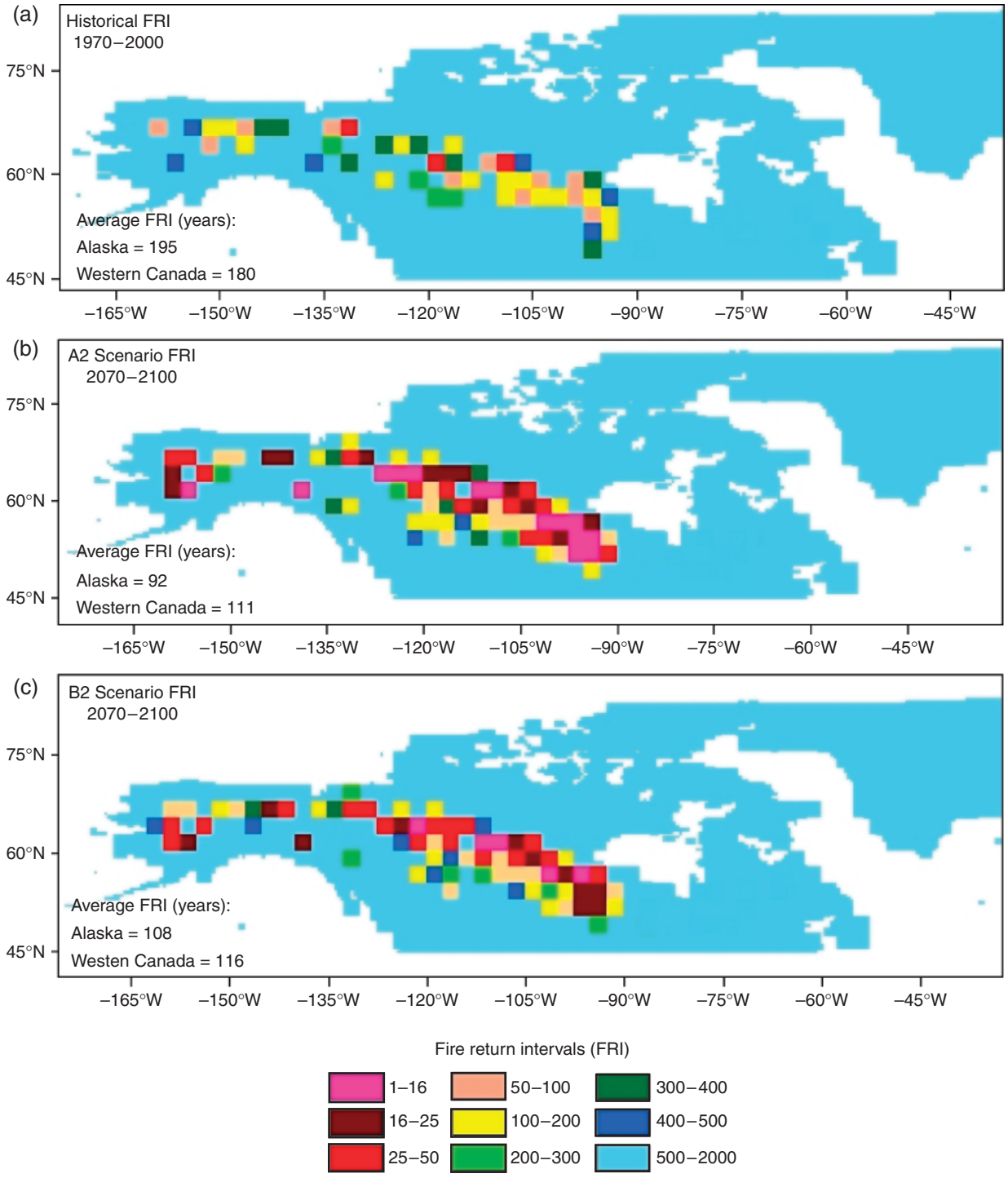


**Fig. 6** Fire return intervals for Alaska and western Canada based on historical fires for years 1970–2000 (a), predicted fires under the A2 scenario for years 2070–2100 (b), and predicted fires under the B2 scenario for years 2070–2100 (c).

slices (e.g. 2080–2100), which preclude their use in our study, which sought to understand changes from the historical fire record through the entire 21st century. Availability of restricted time slices also precludes the direct coupling of fire predictions to biogeochemical models for understanding the role of fire on carbon dynamics for future scenarios of climate change. For these reasons, we were limited to the CGCM2 coupled

ocean–atmosphere GCM. Other issues related to GCM data stem from the calculation of additional variables (e.g. deriving relative humidity from specific humidity) that, in principle, can be obtained but may yield unrealistic values.

Other variables that we did not consider might also influence future fire regime. While we were able to explain about 82% of the variation in annual area burned with models driven by fuel moisture, air temperature, and MSR, other variables such as lightning strikes, fire suppression, and the successional dynamics following fire may help to more accurately predict area burned on an annual basis. Incorporating spatially and temporally explicit lightning ignition information into future analyses could be useful with respect to understanding the initial location and subsequent spread of fire, especially at fine spatial scales. However, the Alaska Fire Service and Canadian lightning strike detection network data have only recently become available (since 1986 for Alaska; 1988 for Canada) and do not have temporal coverage spanning the entire length of the historical fire record. Furthermore, because current GCMs do not incorporate an explicit component that models cloud to ground lightning strike activity, it is not currently possible to obtain this information and include it as an additional predictor variable in modeling studies. Other studies have focused on using satellite data to reconstruct ignition location and fire development, and information from these studies may be useful for developing models to predict future fire threats (Loboda & Csiszar, 2007).

Fire activity in Canada has been increasing since the 1970s (Podur *et al*., 2002; Gillett *et al*., 2004). All things remaining equal, we would expect that area burned would be decreasing due to increased spatial coverage of fire suppression and increased efficiency in fire suppression activities including the use of water bombers (Van Wagner, 1988; Bergeron *et al*., 2004, 2006). There is some debate on the effects of fire suppression over large areas and longer timescales (Miyanishi & Johnson, 2001; Ward *et al*., 2001) but we would expect a decrease in area burned over the short term due to fire management (Cumming, 2005). While fire management agencies operate with a narrow margin between success and failure, a disproportionate number of fires may escape initial attack under a warmer climate, resulting in an increase in area burned much greater than the corresponding increase in fire weather severity (Stocks, 1993). In northern California, Fried *et al*. (2004) used an initial attack model under a $2\times$ $CO_2$ climate scenario and found that increased fire severity produced faster spreading and more intense fires which lead to increases in escape fires by 50–125% over current levels.

Modeling the linkage between climate and fire through empirical relationships limits the potential to incorporate intervening processes. For example, we do not incorporate an available fuels component, which is commonly used in more process-based approaches (see Arora & Boer, 2005). It has been shown that forest composition can influence fire initiation patterns in the boreal forest (Krawchuk *et al*., 2007). In addition, fire-induced changes in the proportion of deciduous stands to conifer stands could alter climate–fire interactions in response to changes in future climate. Increases in the frequency and extent of fire could cause a shift from a conifer-dominated landscape to a deciduous-dominated landscape (Rupp *et al*., 2001), or might cause regional shifts in the distribution of vegetation types. Coupling our area burned estimates to models that simulate successional trajectories and biome shifts in response to fire and climate (e.g. ALFRESCO; see Rupp *et al*., 2002) could provide information with respect to the amount and flammability of fuels across the landscape for future scenarios of climate change.

Finally, future studies should examine the role of future climatic change on the number and sizes of human-caused fires across the boreal region. Wotton *et al*. (2003) suggested that up to a 50% increase in the total number of human-caused fires could be expected in Ontario, Canada, by the end of the 21st century. Incorporating human-caused fires into future wildfire area estimates will give a more complete picture with respect to the influence of future fire on the carbon dynamics of this region.

## Conclusions

The projected changes in climate across high-latitude regions could significantly alter the current wildfire regimes across the North American boreal forest. Our conclusions support previous studies that have shown that changes in climate could cause increased burning (Flannigan *et al*., 2000) and extended fire seasons (Wotton & Flannigan, 1993) in portions of the western boreal forest. These changes in the fire regime have major implications for the carbon dynamics (Zhuang *et al*., 2006; Balshi *et al*., 2007) of this region, as well as potential energy feedbacks to the climate system (Randerson *et al*., 2006) through the influence of altered successional pathways.

The empirical models that we developed in this study have the capability to predict historical area burned for western boreal North America. However, incorporating the effects of changes in vegetation composition and structure on future fire regimes at large spatial scales (e.g. biome shifts) remains a significant challenge that is

 

best addressed by dynamic vegetation model (DVM) development. Several studies have focused on developing methods for incorporating fire into DVMs at global (Thonicke *et al*., 2001; Venevsky *et al*., 2002) and landscape scales (Keane *et al*., 1996; He & Mladenoff, 1999; Rupp *et al*., 2001, 2002). The integration of understanding gained from our study into future DVM development is important for predicting the role of fire in the coupled vegetation–climate system. Together, a more accurate representation of interactions among fire, climate, and vegetation dynamics can improve our ability to predict how carbon and energy exchange of the North America boreal region may change in response to future climate change.

## Acknowledgements

Funding for this study was provided by grants from the National Science Foundation Biocomplexity Program (ATM-0120468) and Office of Polar Programs (OPP-0531047, OPP-0328282, and OPP-0327664), the National Aeronautics and Space Administration North America Carbon Program (NNG05GD25G), and the Bonanza Creek LTER (Long-Term Ecological Research) Program (funded jointly by NSF grant DEB-0423442 and USDA Forest Service, Pacific Northwest Research Station grant PNW01-JV11261952-231). This study was also supported in part by a grant of HPC resources from the Arctic Region Supercomputing Center at the University of Alaska Fairbanks as part of the Department of Defense High Performance Computing Modernization Program.

## References

Amiro BD, Logan KA, Wotton BM, Flannigan MD, Stocks BJ, Martell DL (2004) Fire weather index system components for large fires in the Canadian boreal forest. *International Journal of Wildland Fire*, **13**, 391–400.

Arora VK, Boer GJ (2005) Fire as an interactive component of dynamic vegetation models. *Journal of Geophysical Research*, **110**, G02008, doi: 10.1029/2005JG000042.

Balshi MS, McGuire AD, Zhuang Q *et al*. (2007) The role of historical fire disturbance in the carbon dynamics of the pan-boreal region: a process-based analysis. *Journal of Geophysical Research*, **112**, G02029, doi: 10.1029/2006JG000380.

Bergeron Y, Cyr D, Drever CR *et al*. (2006) Past, current, and future fire frequencies in Quebec's commercial forests: implications for the cumulative effects of harvesting and fire on age-class structure and natural disturbance-based management. *Canadian Journal of Forest Research*, **36**, 2737–2744.

Bergeron Y, Flannigan M, Gauthier S, Leduc A, Lefort P (2004) Past, current, and future fire frequency in the Canadian boreal forest: implications for sustainable forest management. *Ambio*, **33**, 356–360.

Bureau of Land Management, Alaska Fire Service (2005) Alaska Fire History, 1950–2004, Vector Digital Data: http://agdc.usgs.gov/data/blm/fire/index.html

Calef MP, McGuire AD, Chapin FS III (2008) Human influences on wildfire in Alaska from 1988 through 2005: an analysis of the spatial patterns of human impacts. *Earth Interactions*, **12**, 1–17, doi: 10.1175/2007EI220.1.

Campbell ID, Flannigan MD (2000) Long-term perspectives on fire–climate–vegetation relationships in the North American boreal forest. In: *Fire, Climate Change, and Carbon Cycling in the Boreal Forest, Ecological Studies*, Vol. 138 (eds Kasischke ES, Stocks BJ), pp. 152–172. Springer-Verlag, New York.

Carcaillet C, Bergeron Y, Richard PJH, Fréchette B, Gauthier S, Prairie YT (2001) Change of fire frequency in the eastern Canadian boreal forests during the Holocene: does vegetation composition or climate trigger the fire regime? *Journal of Ecology*, **89**, 930–946.

Chambers SD, Chapin FS III (2003) Fire effects on surface–atmosphere exchange in Alaskan black spruce ecosystems: implications for feedbacks to regional climate. *Journal of Geophysical Research*, **108**, 8145, doi: 10.1029/2001JD000530.

Chapin FS III, McGuire AD, Randerson J *et al*. (2000) Arctic and boreal ecosystems of western North America as components of the climate system. *Global Change Biology*, **6** (Suppl. 1), 211–223.

Chapin FS, Rupp TS, Starfield AM *et al*. (2003) Planning for resilience: modeling change in human-fire interactions in the Alaskan boreal forest. *Frontiers in Ecology and the Environment*, **1**, 255–261.

Chapin FS III, Trainor SF, Huntington O *et al*. (2008) Increasing wildfire in Alaska's boreal forest: causes, consequences, and pathways to potential solutions of a wicked problem. *BioScience*, **58**, 531–540.

Clark JS (1990) Effect on climate change on fire regimes in northwestern Minnesota. *Nature*, **334**, 233–235.

Cumming SG (2005) Effective fire suppression in boreal forests. *Canadian Journal of Forest Research*, **35**, 772–786.

De Veaux RD, Gordon AL, Comiso JC, Bacherer NE (1993) Modeling of topographic effects on Antarctic sea ice using multivariate adaptive regression splines. *Journal of Geophysical Research*, **98**, 20307–20320.

Dissing D, Verbyla DL (2003) Spatial patterns of lightning strikes in interior Alaska and their relations to elevation and vegetation. *Canadian Journal of Forest Research*, **33**, 770–782.

Duffy PA, Walsh JE, Graham JM, Mann DH, Rupp TS (2005) Impacts of large-scale atmospheric-ocean variability on Alaskan fire season severity. *Ecological Applications*, **15**, 1317–1330.

Flannigan MD, Bergeron Y, Engelmark O, Wotton BM (1998) Future wildfire in circumboreal forests in relation to global warming. *Journal of Vegetation Science*, **9**, 469–476.

Flannigan MD, Campbell I, Wotton M, Carcaillet C, Richard P, Bergeron Y (2001) Future fire in Canada's boreal forest: paleoecology results and general circulation model – regional climate model simulations. *Canadian Journal of Forest Research*, **31**, 854–864.

Flannigan MD, Harrington JB (1988) A study of the relation of meteorological variables to monthly provincial area burned by wildfire in Canada (1953–80). *Journal of Applied Meteorology*, **27**, 441–452.

Flannigan MD, Logan KA, Amiro BD, Skinner WR, Stocks BJ (2005) Future area burned in Canada. *Climatic Change*, **72**, 1–16.

Flannigan MD, Stocks BJ, Wotton BM (2000) Climate change and forest fires. *The Science of the Total Environment*, **262**, 221–229.

Flannigan MD, Van Wagner CE (1991) Climate change and wildfire in Canada. *Canadian Journal of Forest Research*, **21**, 66–72.

Flato GM, Boer GJ (2000) Warming asymmetry in climate change simulations. *Geophysical Research Letters*, **28**, 195–198.

Fraser RH, Li Z, Cihlar J (2000) Hotspot and NDVI differencing synergy (HANDS): a new technique for burned area mapping over boreal forest. *Remote Sensing of Environment*, **74**, 362–376.

Fried JS, Torn MS, Mill E (2004) The impact of climate change on wildfire severity: a regional forecast for Northern California. *Climate Change*, **64**, 169–191.

Friedman JH (1991) Multivariate adaptive regression splines. *The Annals of Statistics*, **19**, 1–141.

Gillett NP, Weaver AJ, Zwiers FW, Flannigan MD (2004) Detecting the effect of climate change on Canadian forest fires. *Geophysical Research Letters*, **31**, L18211, doi: 10.1029/2004GL020876.

Government of Alberta (2005) Historical Wildfires: 1931–1979, PFFC.GIS@gov.ab.ca, Wildfire Resource Information Section, Forest Protection Division, Sustainable Resource Development, Edmonton, Alberta.

Harrington JB, Flannigan MD, Van Wagner CE (1983) *A study of the relation of components of the Fire Weather Index System to monthly provincial area burned by wildfire in Canada 1953–80*. Canadian Forestry Services, Information Report PI-X-25, Petawawa, National Forestry Institute.

He HS, Mladenoff DJ (1999) Spatially explicit and stochastic simulation of forest-landscape fire disturbance and succession. *Ecology*, **80**, 81–99.

IPCC (2001) *Climate Change 2001: The Scientific Basis. Contribution of Working Group I to the Third Assessment Report of the Intergovernmental Panel on Climate Change* (eds Houghton JT, Ding Y, Griggs DJ *et al.*), p. 572. Intergovernmental Panel on Climate Change, Cambridge University Press.

Johnson EA (1992) *Fire and Vegetation Dynamics: Studies from the North American Boreal Forest*. Cambridge University Press, Cambridge, UK.

Johnson EA, Wowchuk DR (1993) Wildfires in the southern Canadian Rocky Mountains and their relationship to mid-tropospheric anomalies. *Canadian Journal of Forest Research*, **23**, 1213–1222.

Kalnay E, Kanamitsu M, Kistler R *et al.* (1996) The NCEP/NCAR 40-year reanalysis project. *Bulletin of the American Meteorological Society*, **77**, 437–470.

Kasischke E, Christensen NL Jr, Stocks BJ (1995) Fire, global warming, and the carbon balance of boreal forests. *Ecological Applications*, **5**, 437–451.

Kasischke ES, Rupp TS, Verbyla DL (2006) Fire trends in the Alaskan boreal forest. In: *Alaska's Changing Boreal Forest* (eds Chapin FS III, Oswood MW, Van Cleve K, Viereck LA, Verbyla DL), pp. 285–301. Oxford University Press, New York.

Kasischke ES, Williams D, Barry D (2002) Analysis of the patterns of large fires in the boreal forest region of Alaska. *International Journal of Wildland Fire*, **11**, 131–144.

Keane RE, Ryan KC, Running SW (1996) Simulating effects of fire on northern Rocky Mountain landscapes with the ecological process model FIRE-BGC. *Tree Physiology*, **16**, 319–331.

Krawchuk MA, Cumming SG, Flannigan MD, Wein RW (2007) Biotic and abiotic regulation of lightning fire initiation in the mixedwood boreal forest. *Ecology*, **87**, 458–468.

Leathwick JR, Rowe D, Richardson J, Elith J, Hastie T (2005) Using multivariate adaptive regression splines to predict the distributions of New Zealand's freshwater diadromous fish. *Freshwater Biology*, **50**, 2034–2052.

Loboda TV, Csiszar IA (2007) Assessing the risk of ignition in the Russian far east within a modeling framework of fire threat. *Ecological Applications*, **17**, 791–805.

Macias Fauria M, Johnson EA (2006) Large-scale climatic patterns control large lightning fire occurrence in Canada and Alaska forest regions. *Journal of Geophysical Research*, **111**, G04008, doi: 10.1029/2006JG000181.

McCoy VM, Burn CR (2005) Potential alteration by climate change of the forest-fire regime in the boreal forest of Central Yukon Territory. *Arctic*, **58**, 276–285.

McGuire AD, Chapin FS III, Wirth C *et al.* (2007) Responses of high latitude ecosystems to global change: potential consequences for the climate system. In: *Terrestrial Ecosystems in a Changing World* (eds Canadell JG, Pataki DE, Pitelka LF), pp. 297–310. Springer-Verlag, Berlin/Heidelberg, The IGBP Series.

McGuire AD, Wirth C, Apps M *et al.* (2002) Environmental variation, vegetation distribution, carbon dynamics, and water/energy exchange in high latitudes. *Journal of Vegetation Science*, **13**, 301–314.

Miyanishi K, Johnson EA (2001) Comment – a reexamination of the effects of fire suppression in the boreal forest. *Canadian Journal of Forest Research*, **31**, 1462–1466.

Moisen GG, Frescino TS (2002) Comparing five modeling techniques for predicting forest characteristics. *Ecological Modelling*, **157**, 209–225.

Naelapea O, Nickeson J (1998) *SERM Forest Fire Chronology of Saskatchewan in Vector Format*. Oak Ridge National Laboratory Distributed Active Archive Center, Oak Ridge, TN, USA.

Nakićenović N, Swart R (eds) (2000) *Intergovernmental Panel on Climate Change, Special Report on Emissions Scenarios*. Cambridge University Press, Cambridge, UK.

Nash CH, Johnson EA (1996) Synoptic climatology of lightning-caused forest fires in subalpine and boreal forests. *Canadian Journal of Forest Research*, **26**, 1859–1874.

Podur J, Martell DL, Knight K (2002) Statistical quality control analysis of forest fire activity in Canada. *Canadian Journal of Forest Research*, **32**, 195–205.

Randerson JT, Liu H, Flanner MG *et al.* (2006) The impact of boreal forest fire on climate warming. *Science*, **314**, 1130–1132.

Rupp TS, Chapin FS III, Starfield AM (2001) Modeling the influence of topographic barriers on treeline advance of the forest–tundra ecotone in Northwestern Alaska. *Climatic Change*, **48**, 399–416.

Rupp TS, Starfield AM, Chapin FS III, Duffy P (2002) Modeling the impact of black spruce on the fire regime of Alaskan boreal forest. *Climatic Change*, **55**, 213–233.

 

Skinner WR, Flannigan MD, Stocks BJ *et al*. (2002) A 500 h Pa synoptic wildland fire climatology for large Canadian forest fires, 1959–1996. *Theoretical and Applied Climatology*, **71**, 157–169.

Skinner WR, Stocks BJ, Martell DL, Bonsal B, Shabbar A (1999) The association between circulation anomalies in the mid-troposphere and area burned by wildland fire in Canada. *Theoretical and Applied Climatology*, **63**, 89–105.

Stocks BJ (1993) Global warming and forest fires in Canada. *Forestry Chronicle*, **69**, 290–293.

Stocks BJ, Fosberg MA, Lynham TJ *et al*. (1998) Climate change and forest fire potential in Russian and Canadian boreal forests. *Climatic Change*, **38**, 1–13.

Stocks BJ, Mason JA, Todd JB *et al*. (2002) Large forest fires in Canada, 1959–1997. *Journal of Geophysical Research*, **108**, 8149, doi: 10.1029/2001JD000484.

Swetnam TW, Betancourt JL (1990) Fire-southern oscillation relations in the southwestern United States. *Science*, **249**, 1017–1020.

Thonicke K, Venevsky S, Sitch S, Cramer W (2001) The role of fire disturbance for global vegetation dynamics: coupling fire into a dynamic global vegetation model. *Global Ecology & Biogeography*, **10**, 661–677.

Tymstra C, Flannigan MD, Armitage OB, Logan K (2007) Impact of climate change on area burned in Alberta's boreal forest. *International Journal of Wildland Fire*, **16**, 153–160.

Van Wagner CE (1970) *An index to estimate the current moisture content of the forest floor*. Canadian Forest Service, Department of Forestry and Fisheries, publication no. 1288.

Van Wagner CE (1987) *Development and structure of the Canadian Forest Fire Weather Index System*. Canadian Forest Service, Forestry Technical Report 35.

Van Wagner CE (1988) The historical pattern of annual burned area in Canada. *Forestry Chronicle*, **64**, 182–185.

Venevsky S, Thonicke K, Sitch S, Cramer W (2002) Simulating fire regimes in human-dominated ecosystems: Iberian Peninsula case study. *Global Change Biology*, **8**, 984–998.

Ward PC, Tithecott AG, Wotton BM (2001) Reply – a re-examination of the effects of fire suppression in the boreal forest. *Canadian Journal of Forest Research*, **31**, 1467–1480.

Weber MG, Flannigan MD (1997) Canadian boreal forest ecosystem structure and function in a changing climate: impact on fire regimes. *Environmental Review*, **5**, 145–166.

Westerling AL, Hidalgo HG, Cayan DR, Swetnam TW (2006) Warming and earlier spring increases western U.S. forest wildfire activity. *Science*, **313**, 940–843.

Wilmore B (2001) *Duff moisture dynamics in black spruce feather moss stands and their relation to the Canadian forest fire danger rating system*. MS thesis, University of Alaska Fairbanks, 117 pp.

Wotton BM, Flannigan MD (1993) Length of the fire season in a changing climate. *Forestry Chronicle*, **69**, 187–192.

Wotton BM, Martell DL, Logan KA (2003) Climate change and people-caused forest fire occurrence in Ontario. *Climatic Change*, **60**, 275–295.

Zhuang Q, Melillo JM, Felzer BS *et al*. (2006) $CO_2$ and $CH_4$ exchanges between land ecosystems and the atmosphere in northern high latitudes over the 21st century. *Geophysical Research Letters*, **33**, L17403, doi: 10.1029/2006GL026972.

## Appendix A

**Table A1** Multivariate Adaptive Regression Spline (MARS) models and associated basis functions listed by spatial location. Location corresponds to the lower left hand corner of each 2.5° grid cell

| Location | Model |
|---|---|
| 65W, 52.5N | $Y = \max(0, 2.692 + 1314.078 \times BF3)$ |
| | $BF1 = \max(0, DCJULY - 37.187)$ |
| | $BF3 = \max(0, 0.300000E\text{-}03 - MSRJUNE) \times BF1$ |
| 67.5W, 52.5N | $Y = \max(0, 34.447 + 9449.171 \times BF1)$ |
| | $BF1 = \max(0, MSRJULY + 0.564563E\text{-}10)$ |
| 72.5W, 50N | $Y = \max(0, 7.635 + 116393.727 \times BF8)$ |
| | $BF8 = \max(0, MSRJUNE - 0.300000E\text{-}03)$ |
| 72.5W, 52.5N | $Y = \max(0, -15.499 + 1.217 \times BF9 + 42.377 \times BF18)$ |
| | $BF9 = \max(0, DCJULY - 148.781)$ |
| | $BF18 = \max(0, TEMPJULY - 11.993)$ |
| 75W, 47.5N | $Y = \max(0, -54.370 + 282.784 \times BF1)$ |
| | $BF1 = \max(0, DMCJUNE - 0.230)$ |
| 75W, 50N | $Y = \max(0, 8.710 + 20312.041 \times BF1 + 1891.058 \times BF4)$ |
| | $BF1 = \max(0, MSRAUG - 0.600000E\text{-}03)$ |
| | $BF4 = \max(0, 0.287 - DMCMAY)$ |
| 75W, 52.5N | $Y = \max(0, 45.326 + 5.356 \times BF1)$ |
| | $BF1 = \max(0, DCAUG - 194.548)$ |
| 77.5W, 47.5N | $Y = \max(0, 19.448 + 7.991 \times BF21$ |
| | $BF21 = \max(0, FFMCJUNE - 38.283)$ |
| 77.5W, 52.5N | $Y = \max(0, 64.709 + 22.090 \times BF1)$ |
| | $BF1 = \max(0, DCAUG - 259.319)$ |
| 80W, 47.5N | $Y = \max(0, 25.683 + 12.619 \times BF7)$ |
| | $BF7 = \max(0, FFMCAUG - 60.823)$ |
| 80W, 50N | $Y = \max(0, 14.305 + 75.321 \times BF2 + 8.835 \times BF3)$ |
| | $BF2 = \max(0, 6.061 - TEMPMAY)$ |
| | $BF3 = \max(0, DCMAY - 61.274)$ |
| 80W, 52.5N | $Y = \max(0, -8.242 + 15.303 \times BF1)$ |
| | $BF1 = \max(0, DCAUG - 274.942)$ |
| 82.5W, 45N | $Y = \max(0, -3.860 + 16.655 \times BF1 - 1385.199 \times BF8 + 765.408 \times BF10)$ |
| | $BF1 = \max(0, MSRJUNE - 0.006)$ |
| | $BF8 = \max(0, MSRMAY - 0.043)$ |
| | $BF10 = \max(0, MSRMAY - 0.064)$ |
| 82.5W, 47.5N | $Y = \max(0, -28.142 + 8.910 \times BF1 + 9.189 \times BF3 + 695.768 \times BF5)$ |
| | $BF1 = \max(0, DMCJUNE - 0.367)$ |
| | $BF3 = \max(0, 7.964 - TEMPMAY)$ |
| | $BF5 = \max(0, 0.038 - MSRJUNE)$ |
| 82.5W, 50N | $Y = \max(0, -57.475 + 43.509 \times BF2 + 61.148 \times BF5 + 33202.270 \times BF8 + 41.718 \times BF12 + 16.708 \times BF19)$ |
| | $BF2 = \max(0, TEMPAPRI - 2.890)$ |
| | $BF5 = \max(0, TEMPJUNE - 13.697)$ |
| | $BF8 = \max(0, 0.002 - MSRJUNE)$ |
| | $BF12 = \max(0, 2.230 - DMCAPRIL)$ |
| | $BF19 = \max(0, TEMPAUG - 14.916)$ |

*Continued*

**Table A1.** (*Contd.*)

| Location | Model |
|---|---|
| 85W, 47.5N | $Y = \max(0, -1.187 + 364.088 \times BF1 + 17.542 \times BF3)$<br>BF1 = max(0, MSRMAY−0.491275E-09)<br>BF3 = max(0, 1.307−TEMPAPRI) |
| 87.5W, 47.5N | $Y = \max(0, -11.579 + 44.028 \times BF3 + 42.080 \times BF4 + 221.875 \times BF15)$<br>BF3 = max(0, 2.057−TEMPAPRI)<br>BF4 = max(0, TEMPSEPT−14.377)<br>BF15 = max(0, MSRMAY−0.047) |
| 87.5W, 50N | $Y = \max(0, -4.899 + 158.199 \times BF2 + 19.599 \times BF3)$<br>BF2 = max(0,−1.660−TEMPAPRI)<br>BF3 = max(0, FFMCAUG−61.074) |
| 87.5W, 52.5N | $Y = \max(0, 2.283 + 282.371 \times BF1)$<br>BF1 = max(0, MSRAUG + 0.305807E-08) |
| 90W, 50N | $Y = \max(0, -7.181 + 2.238 \times BF1 + 79.287 \times BF4 + 70.789 \times BF6)$<br>BF1 = max(0, DCJULY−196.600)<br>BF4 = max(0,−1.013−TEMPAPRI)<br>BF6 = max(0, 16.152−TEMPJULY) |
| 92.5W, 47.5N | $Y = \max(0, -9.871 + 83.208 \times BF2 + 337.940 \times BF3)$<br>BF2 = max(0, 2.187−TEMPAPRI)<br>BF3 = max(0, MSRMAY−0.078) |
| 92.5W, 50N | $Y = \max(0, -128.762 + 3978.068 \times BF1 + 1.776 \times BF15)$<br>BF1 = max(0, MSRJUNE −0.566064E-09)<br>BF15 = max(0, DCAUG−144.552) |
| 92.5W, 52.5N | $Y = \max(0, -34.891 + 3.153 \times BF1 + 160.570 \times BF4)$<br>BF1 = max(0, DCMAY−15.093)<br>BF4 = max(0, TEMPJUNE−14.720) |
| 95W, 47.5N | $Y = \max(0, -42.907 + 297.328 \times BF1 + 313.240 \times BF2 + 1.474 \times BF3 + 57.445 \times BF5)$<br>BF1 = max(0, MSRMAY−0.135)<br>BF2 = max(0, 0.135−MSRMAY)<br>BF3 = max(0, DCJUNE−177.180)<br>BF5 = max(0, MSRJULY−0.001) |
| 95W, 50N | $Y = \max(0, -205.171 + 845.936 \times BF1 + 4.494 \times BF3 + 7.441 \times BF4)$<br>BF1 = max(0, TEMPJULY−19.884)<br>BF3 = max(0, DCJUNE−115.090)<br>BF4 = max(0, 115.090−DCJUNE) |
| 95W, 52.5N | $Y = \max(0, -22.889 + 284.661 \times BF1 + 305.591 \times BF3 + 100.778 \times BF5)$<br>BF1 = max(0, TEMPJUNE−15.700)<br>BF3 = max(0, TEMPJULY−18.594)<br>BF5 = max(0, TEMPMAY−8.871) |
| 95W, 55N | $Y = \max(0, -24.846 + 486.335 \times BF1 + 45601.629 \times BF4)$<br>BF1 = max(0, TEMPJULY−17.294)<br>BF4 = max(0, 0.004−MSRAPRIL) |
| 97.5W, 47.5N | $Y = \max(0, 12.417 + 2.108 \times BF1)$<br>BF1 = max(0, DCMAY−112.958) |
| 97.5W, 50N | $Y = \max(0, -94.648 + 1892.714 \times BF1 + 502.313 \times BF2 + 352.734 \times BF4 + 119.890 \times BF5)$<br>BF1 = max(0, MSRAPRIL−0.699998E-03)<br>BF2 = max(0, TEMPJULY−21.110)<br>BF4 = max(0, MSRMAY−0.363630E-08)<br>BF5 = max(0, TEMPJUNE−17.460) |
| 97.5W, 52.5N | $Y = \max(0, 36.779 + 800.542 \times BF1)$<br>BF1 = max(0, TEMPJULY−19.613) |
| 97.5W, 55N | $Y = \max(0, 57.223 + 1414.958 \times BF1)$<br>BF1 = max(0, TEMPJULY−17.852) |
| 100W, 50N | $Y = \max(0, -31.976 + 62.135 \times BF1 + 68.646 \times BF2 \times BF3)$<br>BF1 = max(0, DMCJUNE−9.710)<br>BF2 = max(0, TEMPJULY−19.839)<br>BF3 = max(0, 9.710−DMCJUNE) |
| 100W, 52.5N | $Y = \max(0, -31.312 + 537.808 \times BF1 + 3.517 \times BF2)$<br>BF1 = max(0, MSRJULY−0.655)<br>BF2 = max(0, DCJULY−318.332) |
| 100W, 55N | $Y = \max(0, -1291.159 + 4.343 \times BF2 + 887.734 \times BF3 + 209.611 \times BF4 + 5.834 \times BF5 + 864.193 \times BF6 + 971.245 \times BF7)$<br>BF2 = max(0, 339.671−DCAUG)<br>BF3 = max(0, TEMPJULY−18.061)<br>BF4 = max(0, 18.061−TEMPJULY)<br>BF5 = max(0, DCJULY−121.881)<br>BF6 = max(0, MSRSEPT−0.002)<br>BF7 = max(0, MSRJUNE −0.700000E-03) |
| 100W, 57.5N | $Y = \max(0, -83.796 + 5805.285 \times BF1 + 5023.921 \times BF3)$<br>BF1 = max(0, MSRJULY−0.076)<br>BF3 = max(0, MSRSEPT−0.046) |
| 102.5W, 50N | $Y = \max(0, -203.056 + 43.121 \times BF1 + 20.587 \times BF2 + 1.984 \times BF3)$<br>BF1 = max(0, DMCJUNE−10.503)<br>BF2 = max(0, 10.503−DMCJUNE)<br>BF3 = max(0, DCMAY−35.210) |
| 102.5W, 52.5N | $Y = \max(0, -24.705 + 434.277 \times BF1 + 478.899 \times BF3)$<br>BF1 = max(0, MSRJULY−0.670)<br>BF3 = max(0, MSRMAY−0.020) |
| 102.5W, 55N | $Y = \max(0, -2220.454 + 1250.298 \times BF1 + 270.639 \times BF2 + 89.393 \times BF3 + 18.598 \times BF4 + 47.616 \times BF7 + 63295.504 \times BF9)$<br>BF1 = max(0, TEMPJULY−17.797)<br>BF2 = max(0, 17.797−TEMPJULY)<br>BF3 = max(0, DMCJUNE−0.740)<br>BF4 = max(0, FFMCSEPT−38.600) |

*Continued*

 

**Table A1.** (*Contd.*)

| Location | Model |
|---|---|
| | BF7 = max(0, FFMCAPRI−37.883) |
| | BF9 = max(0, 0.015−MSRAPRIL) |
| 102.5W, 57.5N | $Y$ = max(0, −126.101 + 2747.822 × BF1 + 233.166 × BF3 + 28.128 × BF5) |
| | BF1 = max(0, MSRSEPT−0.035) |
| | BF3 = max(0, TEMPJULY−15.297) |
| | BF5 = max(0, TEMPAPRI + 8.493) |
| 105W, 52.5N | $Y$ = max(0, −304.954 + 130.275 × BF1 + 60.349 × BF3 + 43.616 × BF4 + 50.088 × BF5 + 57.388 × BF12) |
| | BF1 = max(0, MSRAUG−1.149) |
| | BF3 = max(0, TEMPJUNE−11.670) |
| | BF4 = max(0, TEMPAPRI−0.967) |
| | BF5 = max(0, 0.967−TEMPAPRI) |
| | BF12 = max(0, 18.539−TEMPAUG) |
| 105W, 55N | $Y$ = max(0, 171.338 + 150.583 × BF2) |
| | BF2 = max(0, 22.083−DCAPRIL) |
| 105W, 57.5N | $Y$ = max(0, −548.324 + 14951.786 × BF3 + 226.436 × BF4 + 157.459 × BF5) |
| | BF3 = max(0, MSRAPRIL + 0.128952E-09) |
| | BF4 = max(0, TEMPJULY−12.223) |
| | BF5 = max(0, FFMCAUG−62.787) |
| 105W, 60N | $Y$ = max(0, −254.888 + 2913.429 × BF2 + 213.817 × BF3 + 2596.765 × BF18) |
| | BF2 = max(0, 0.090−MSRAUG) |
| | BF3 = max(0, TEMPJULY−14.355) |
| | BF18 = max(0, MSRAUG−0.010) |
| 107.5W, 52.5N | $Y$ = max(0, −81.741 + 12.452 × BF3 + 7.123 × BF4 + 0.894 × BF5 + 16.283 × BF7) |
| | BF3 = max(0, FFMCSEPT−72.220) |
| | BF4 = max(0, 72.220−FFMCSEPT) |
| | BF5 = max(0, DCJULY−279.303) |
| | BF7 = max(0, FFMCMAY−68.681) |
| 107.5W, 55N | $Y$ = max(0, −13.193 + 34.389 × BF3 + 2.155 × BF8) |
| | BF3 = max(0, DMCJUNE−0.820) |
| | BF8 = max(0, DCSEPT−365.537) |
| 107.5W, 57.5N | $Y$ = max(0, −411.566 + 14737.769 × BF1 + 54324.848 × BF2 + 93.209 × BF3 + 25.552 × BF5) |
| | BF1 = max(0, MSRAPRIL−0.010) |
| | BF2 = max(0, 0.010−MSRAPRIL) |
| | BF3 = max(0, FFMCSEPT−62.563) |
| | BF5 = max(0, FFMCJUNE−35.497) |
| 107.5W, 60N | $Y$ = max(0, −9.153 + 617.092 × BF1 + 737.360 × BF3) |
| | BF1 = max(0, TEMPJULY−15.668) |
| | BF3 = max(0, MSRJULY−0.806750E-10) |
| 110W, 52.5N | $Y$ = max(0, 27.357 + 5.554 × BF1) |
| | BF1 = max(0, DCJULY−347.845) |

*Continued*

**Table A1.** (*Contd.*)

| Location | Model |
|---|---|
| 110W, 55N | $Y$ = max(0, −549.253 + 133.138 × BF2 + 40.932 × BF3 + 5.406 × BF6 + 12.582 × BF13 + 29293.217 × BF15) |
| | BF2 = max(0, 53.742−FFMCAUG) |
| | BF3 = max(0, DMCJUNE−0.687) |
| | BF6 = max(0, DCSEPT−409.260) |
| | BF13 = max(0, 199.273−DCJUNE) |
| | BF15 = max(0, 0.021−MSRAPRIL) |
| 110W, 57.5N | $Y$ = max(0, −578.903 + 78963.859 × BF2 + 37332.512 × BF14) |
| | BF2 = max(0, 0.017−MSRAPRIL) |
| | BF14 = max(0, MSRAPRIL−0.004) |
| 110W, 60N | $Y$ = max(0, −372.184 + 8674.142 × BF1 + 409.678 × BF12) |
| | BF1 = max(0, MSRSEPT−0.072) |
| | BF12 = max(0, TEMPJULY−14.871) |
| 112.5W, 52.5N | $Y$ = max(0, −23.827 + 33.411 × BF1 + 7.589 × BF2 + 0.436 × BF4 + 236.183 × BF5) |
| | BF1 = max(0, TEMPAPRI−3.903) |
| | BF2 = max(0, 3.903−TEMPAPRI) |
| | BF4 = max(0, 332.977−DCSEPT) |
| | BF5 = max(0, MSRAPRIL−0.999997E-03) |
| 112.5W, 55N | $Y$ = max(0, −26.734 + 39.066 × BF1) |
| | BF1 = max(0, DMCJUNE−0.580) |
| 112.5W, 57.5N | $Y$ = max(0, 215.883 + 742.065 × BF1 + 225.569 × BF3−66.951 × BF5 + 47.767 × BF7) |
| | BF1 = max(0, TEMPAUG−16.852) |
| | BF3 = max, (0, FFMCAPRI−67.870) |
| | BF5 = max(0, FFMCAPRI−53.967) |
| | BF7 = max(0DMCSEPT−4.283) |
| 112.5W, 60N | $Y$ = max(0, 78.188 + 1231.887 × BF1) |
| | BF1 = max(0, TEMPJULY−17.132) |
| 112.5W, 62.5N | $Y$ = max(0, −7.636 + 212.035 × BF1 + 236.977 × BF10) |
| | BF1 = max(0, MSRJULY−0.680) |
| | BF10 = max(0, MSRSEPT−0.030) |
| 115W, 47.5N | $Y$ = max(0, −0.585 + 0.045 × BF1 + 1.112 × BF3 + 0.502 × BF5 |
| | BF1 = max(0, DCAUG−426.555) |
| | BF3 = max(0, TEMPJULY−17.048) |
| | BF5 = max(0, FFMCAUG−83.439) |
| 115W, 52.5N | $Y$ = max(0, 185.396−1151.687 × BF3−403.731 × BF4 + 22694.453 × BF6 + 1203.894 × BF7 + 6311.835 × BF14) |
| | BF3 = max(0, DMCJUNE−2.383) |
| | BF4 = max(0, 2.383−DMCJUNE) |
| | BF6 = max(0, 0.019−MSRJUNE) |
| | BF7 = max(0, DMCJUNE−2.773) |
| | BF14 = max(0, 0.027−MSRAUG) |
| 115W, 55N | $Y$ = max(0, 43.668 + 4.303 × BF16) |
| | BF16 = max(0, DCAUG−376.123) |

*Continued*

**Table A1.** (*Contd.*)

| Location | Model |
|---|---|
| 115W, 57.5N | $Y = \max(0, -54.613 + 574.023 \times BF3 + 6213.206 \times BF19)$<br>$BF3 = \max(0, TEMPAUG - 17.161)$<br>$BF19 = \max(0, MSRAPRIL - 0.011)$ |
| 115W, 60N | $Y = \max(0, 16.029 + 324.355 \times BF1 + 6618.464 \times BF3$<br>$BF1 = \max(0, TEMPAUG - 16.987)$<br>$BF3 = \max(0, MSRAPRIL - 0.020)$ |
| 115W, 62.5N | $Y = \max(0, -9.330 + 551.633 \times BF1 + 24.723 \times BF18)$<br>$BF1 = \max(0, TEMPJULY - 16.965)$<br>$BF18 = \max(0, DCMAY - 80.429)$ |
| 117.5W, 50N | $Y = \max(0, -31.660 + 27.374 \times BF2 - 227.389 \times BF3 + 14488.044 \times BF6 + 238.291 \times BF15)$<br>$BF2 = \max(0, 7.077 - TEMPSEPT)$<br>$BF3 = \max(0, MSRJULY - 0.241)$<br>$BF6 = \max(0, 0.003 - MSRJUNE)$<br>$BF15 = \max(0, MSRJULY - 0.074)$ |
| 117.5W, 52.5N | $Y = \max(0, -16.168 + 27.913 \times BF1 + 95.058 \times BF5)$<br>$BF1 = \max(0, DMCSEPT - 4.973)$<br>$BF5 = \max(0, TEMPMAY - 3.977)$ |
| 117.5W, 55N | $Y = \max(0, -7.520 + 56.752 \times BF1 + 43.487 \times BF4 + 420.004 \times BF5)$<br>$BF1 = \max(0, TEMPJUNE - 11.727)$<br>$BF4 = \max(0, 0.077 - TEMPAPRI)$<br>$BF5 = \max(0, MSRJUNE - 0.120)$ |
| 117.5W, 57.5N | $Y = \max(0, 82.382 + 11.487 \times BF1)$<br>$BF1 = \max(0, DCJULY - 386.023)$ |
| 117.5W, 60N | $Y = \max(0, -169.191 + 116052.242 \times BF2 + 156.086 \times BF4)$<br>$BF2 = \max(0, 0.006 - MSRAPRIL)$<br>$BF4 = \max(0, TEMPMAY - 6.632)$ |
| 117.5W, 62.5N | $Y = \max(0, -14.839 + 497.510 \times BF1 + 117.188 \times BF4 + 139.758 \times BF5)$<br>$BF1 = \max(0, TEMPJULY - 17.203)$<br>$BF4 = \max(0, -6.177 - TEMPAPRI)$<br>$BF5 = \max(0, TEMPSEPT - 8.373)$ |
| 117.5W, 65N | $Y = \max(0, -29.564 + 285.071 \times BF1 + 0.444 \times BF3 + 9.651 \times BF5)$<br>$BF1 = \max(0, MSRSEPT - 0.087)$<br>$BF3 = \max(0, DCJULY - 266.239)$<br>$BF5 = \max(0, 4.826 - DMCAUG)$ |
| 120W, 50N | $Y = \max(0, 0.034 + 31.576 \times BF1 + 26.000 \times BF3)$<br>$BF1 = \max(0, TEMPAUG - 14.381)$<br>$BF3 = \max(0, MSRJULY - 0.120340E\text{-}07)$ |
| 120W, 52.5N | $Y = \max(0, -1.440 + 5.112 \times BF3 + 43.522 \times BF5 + 4.834 \times BF7 + 0.093 \times BF17)$<br>$BF3 = \max(0, TEMPJUNE - 7.193)$<br>$BF5 = \max(0, MSRJULY - 0.012)$<br>$BF7 = \max(0, TEMPAUG - 11.652)$<br>$BF17 = \max(0, 142.810 - DCJULY)$ |

*Continued*

**Table A1.** (*Contd.*)

| Location | Model |
|---|---|
| 120W, 55N | $Y = \max(0, 0.012 + 275.859 \times BF1)$<br>$BF1 = \max(0, TEMPAPRI - 1.447)$ |
| 120W, 57.5N | $Y = \max(0, -19.033 + 84.265 \times BF1 + 12.206 \times BF4 + 49.972 \times BF10)$<br>$BF1 = \max(0, TEMPAUG - 15.807)$<br>$BF4 = \max(0, 55.367 - FFMCAPRI)$<br>$BF10 = \max(0, TEMPMAY - 7.997)$ |
| 120W, 60N | $Y = \max(0, -112.038 + 30759.729 \times BF7 + 4318.878 \times BF9)$<br>$BF7 = \max(0, MSRAPRIL - 0.008)$<br>$BF9 = \max(0, MSRJUNE - 0.302)$ |
| 120W, 62.5N | $Y = \max(0, -664.354 + 1148.508 \times BF1 + 2708.429 \times BF3 + 3602.749 \times BF4 + 16.967 \times BF5 + 13.570 \times BF7 + 330.752 \times BF9 + 2687.791 \times BF12 - 503.358 \times BF16)$<br>$BF1 = \max(0, TEMPJULY - 16.929)$<br>$BF3 = \max(0, MSRJUNE - 0.103)$<br>$BF4 = \max(0, 0.103 - MSRJUNE)$<br>$BF5 = \max(0, DCJULY - 384.523)$<br>$BF7 = \max(0, DCSEPT - 577.560)$<br>$BF9 = \max(0, TEMPSEPT - 8.457)$<br>$BF12 = \max(0, 0.186 - MSRSEPT)$<br>$BF16 = \max(0, TEMPJUNE - 13.497)$ |
| 120W, 65N | $Y = \max(0, 11.578 + 48.703 \times BF5)$<br>$BF5 = \max(0, TEMPJULY - 14.523)$ |
| 122.5W, 52.5N | $Y = \max(0, -7.078 + 527.881 \times BF1 + 33.652 \times BF2)$<br>$BF1 = \max(0, MSRAUG + 0.154813E\text{-}08)$<br>$BF2 = \max(0, TEMPJUNE - 7.677)$ |
| 122.5W, 55N | $Y = \max(0, 26.693 + 0.756 \times BF4 + 24.028 \times BF5)$<br>$BF1 = \max(0, TEMPJULY - 11.397)$<br>$BF4 = \max(0, 189.410 - DCJULY) \times BF1$<br>$BF5 = \max(0, TEMPAUG - 13.126) \times BF1$ |
| 122.5W, 60N | $Y = \max(0, 10.112 + 709.577 \times BF1)$<br>$BF1 = \max(0, TEMPSEPT - 9.080)$ |
| 122.5W, 62.5N | $Y = \max(0, -53.670 + 2342.579 \times BF1 + 3.807 \times BF4 - 735.708 \times BF6 + 5013.730 \times BF8)$<br>$BF1 = \max(0, TEMPJULY - 15.493)$<br>$BF4 = \max(0, DCAUG - 437.239)$<br>$BF6 = \max(0, TEMPJULY - 14.777)$<br>$BF8 = \max(0, MSRJUNE - 0.036)$ |
| 122.5W, 65N | $Y = \max(0, -33.329 + 377.958 \times BF10 + 0.782 \times BF13 - 0.500 \times BF14)$<br>$BF10 = \max(0, 0.099 - MSRJULY)$<br>$BF13 = \max(0, DCAUG - 308.061)$<br>$BF14 = \max(0, DCSEPT - 336.347)$ |
| 125W, 52.5N | $Y = \max(0, 4.296 + 549.942 \times BF1)$<br>$BF1 = \max(0, MSRAUG - 0.008)$ |
| 125W, 55N | $Y = \max(0, -2.790 + 2092.266 \times BF1 + 9.695 \times BF2 + 54.186 \times BF7)$ |

*Continued*

 

**Table A1.** (*Contd.*)

| Location | Model |
|---|---|
| | BF1 = max(0, MSRJULY−0.111872E-09) |
| | BF2 = max(0, TEMPAUG−10.861) |
| | BF7 = max(0, 0.400−DMCSEPT) |
| 125W, 57.5N | $Y$ = max(0, −30.978 + 0.779 × BF1 + 221.309 × BF4 + 41194.836 × BF6) |
| | BF1 = max(0, DCAUG−255.929) |
| | BF4 = max(0, 0.563−DMCJUNE) |
| | BF6 = max(0, 0.001−MSRMAY) |
| 125W, 60N | $Y$ = max(0, −452.895 + 2.344 × BF1 + 6.828 × BF3 + 3708.129 × BF13 + 9.575 × BF14) |
| | BF1 = max(0, DCAUG−407.019) |
| | BF3 = max(0, FFMCMAY−30.352) |
| | BF13 = max(0, 0.057−MSRSEPT) |
| | BF14 = max(0, FFMCSEPT−26.063) |
| 125W, 62.5N | $Y$ = max(0, −1264.668 + 709.783 × BF1 + 30160.254 × BF4 + 30.960 × BF5 + 560.206 × BF8 + 128.881 × BF9 + 50.675 × BF12−14.431 × BF15) |
| | BF1 = max(0, TEMPJUNE−10.180) |
| | BF4 = max(0, 0.015−MSRJUNE) |
| | BF5 = max(0, DCAUG−440.003) |
| | BF8 = max(0, TEMPSEPT−5.493) |
| | BF9 = max(0, 5.493−TEMPSEPT) |
| | BF12 = max(0, DCAPRIL−5.820) |
| | BF15 = max(0, DCAUG−404.358) |
| 125W, 65N | $Y$ = max(0, −11.055 + 29.840 × BF1 + 1.943 × BF4) |
| | BF1 = max(0, DMCJULY−5.245) |
| | BF4 = max(0, 357.981−DCAUG) |
| 127.5W, 55N | $Y$ = max(0, −2.304 + 349392.094 × BF2 + 144999.281 × BF4 + 7349344.500 × BF5) |
| | BF1 = max(0, MSRAUG−0.250340E-10) |
| | BF2 = max(0, MSRJULY + 0.306515E-10) × BF1 |
| | BF3 = max(0, MSRAPRIL + 0.345107E-09) |
| | BF4 = max(0, MSRMAY−0.600000E-03) × BF3 |
| | BF5 = max(0, 0.600000E-03−MSRMAY) × BF3 |
| 127.5W, 57.5N | $Y$ = max(0, −42.072 + 11501.986 × BF1 + 4.536 × BF3 + 89.207 × BF5) |
| | BF1 = max(0, MSRAPRIL−0.009) |
| | BF3 = max(0, DCSEPT−360.953) |
| | BF5 = max(0, DMCJUNE−0.723) |
| 127.5W, 60N | $Y$ = max(0, 20.158 + 1.583 × BF3) |
| | BF1 = max(0, DCJULY−257.645) |
| | BF3 = max(0, TEMPJULY−6.306) × BF1 |
| 127.5W, 62.5N | $Y$ = max(0, −344.948 + 214.326 × BF1 + 266.348 × BF7 + 10.813 × BF8 + 215.752 × BF18) |
| | BF1 = max(0, TEMPMAY−1.990) |
| | BF7 = max(0, 10.761−TEMPJULY) |
| | BF8 = max(0, DCJULY−294.245) |
| | BF18 = max(0, TEMPJULY−9.800) |
| 127.5W, 65N | $Y$ = max(0, 61.503 + 275.888 × BF1) |
| | BF1 = max(0, DCAPRIL−22.230) |
| 130W, 57.5N | $Y$ = max(0, −145.141 + 14.729 × BF1 + 5.735 × BF2 + 6.038 × BF4 + 3.381 × BF6 + 6291.277 × BF8) |
| | BF1 = max(0, FFMCJUNE−45.143) |
| | BF2 = max(0, 45.143−FFMCJUNE) |
| | BF4 = max(0, FFMCSEPT−26.843) |
| | BF6 = max(0, DCJULY−251.174) |
| | BF8 = max(0, MSRAPRIL−0.011) |
| 130W, 60N | $Y$ = max(0, −120.089 + 77.844 × BF1 + 121.595 × BF2 + 7067.656 × BF3 + 36.058 × BF8 + 3.117 × BF10) |
| | BF1 = max(0, TEMPJULY−8.184) |
| | BF2 = max(0, 8.184−TEMPJULY) |
| | BF3 = max(0, MSRAPRIL−0.011) |
| | BF8 = max(0, − 6.207−TEMPAPRI) |
| | BF10 = max(0, 52.610−FFMCAUG) |
| 130W, 65N | $Y$ = max(0, −779.663 + 11414.481 × BF1 + 532.687 × BF3 + 28.231 × BF5 + 136.821 × BF8 + 104.526 × BF10) |
| | BF1 = max(0, MSRJUNE−0.017) |
| | BF3 = max(0, DCAPRIL−22.143) |
| | BF5 = max(0, FFMCJULY−46.532) |
| | BF8 = max(0, 6.364−DMCJULY) |
| | BF10 = max(0, TEMPMAY + 0.129) |
| 132.5W, 57.5N | $Y$ = max(0, 1.600 + 9.041 × BF1 + 29.740 × BF3−3.067 × BF5 |
| | BF1 = max(0, FFMCMAY−47.768) |
| | BF3 = max(0, TEMPJUNE−7.767) |
| | BF5 = max(0, FFMCMAY−40.516) |
| 132.5W, 60N | $Y$ = max(0, −39.327 + 5.941 × BF1 + 52.576 × BF5) |
| | BF1 = max(0, DCAUG−433.606) |
| | BF5 = max(0, TEMPAPRI + 5.057) |
| 132.5W, 62.5N | $Y$ = max(0, −84.355 + 48.232 × BF2 + 45.496 × BF8) |
| | BF2 = max(0, 8.055−TEMPAUG) |
| | BF8 = max(0, TEMPAUG−6.342) |
| 132.5W, 65N | $Y$ = max(0, −87.901 + 53.018 × BF5 + 175.081 × BF8) |
| | BF5 = max(0, DMCJULY−0.316) |
| | BF8 = max(0, TEMPAPRI + 7.100) |
| 135W, 57.5N | $Y$ = max(0, 10.901 + 221.731 × BF1−149.745 × BF5) |
| | BF1 = max(0, DMCMAY−0.784) |
| | BF5 = max(0, DMCMAY−0.661) |
| 135W, 60N | $Y$ = max(0, −5.522−4919.515 × BF2 + 69.287 × BF4 + 3841.793 × BF6) |
| | BF2 = max(0, DMCAPRIL−6.013) |
| | BF4 = max(0, DCAPRIL−24.463) |
| | BF6 = max(0, DMCAPRIL−6.000) |
| 135W, 62.5N | $Y$ = max(0, 62.129 + 170.100 × BF1) |
| | BF1 = max(0, TEMPAUG−8.000) |

*Continued*

**Table A1.** (*Contd.*)

| Location | Model |
|---|---|
| 135W, 65N | $Y = \max(0, 65.846 + 100.220 \times BF1)$<br>$BF1 = \max(0, FFMCAPRI - 64.100)$ |
| 137.5W, 60N | $Y = \max(0, 7.761 + 136.466 \times BF1)$<br>$BF1 = \max(0, DCAPRIL - 24.883)$ |
| 137.5W, 62.5N | $Y = \max(0, -52.037 + 146.903 \times BF1 + 307.122 \times BF3 + 11.594 \times BF17)$<br>$BF1 = \max(0, TEMPJUNE - 6.140)$<br>$BF3 = \max(0, TEMPAPRI + 5.253)$<br>$BF17 = \max(0, FFMCJUNE - 37.153)$ |
| 137.5W, 65N | $Y = \max(0, -39.259 + 29.910 \times BF1 + 2963.431 \times BF3 + 125766.211 \times BF4)$<br>$BF1 = \max(0, TEMPAUG - 8.500)$<br>$BF3 = \max(0, MSRJUNE - 0.700000E\text{-}03)$<br>$BF4 = \max(0, 0.700000E\text{-}03 - MSRJUNE)$ |
| 140W, 60N | $Y = \max(0, -2.381 + 16150.373 \times BF1 + 37.651 \times BF2)$<br>$BF1 = \max(0, MSRJUNE + 0.313671E\text{-}10)$<br>$BF2 = \max(0, TEMPSEPT - 5.390)$ |
| 140W, 62.5N | $Y = \max(0, 27.592 + 7.659 \times BF1 + 116.217 \times BF3)$<br>$BF1 = \max(0, DCJULY - 281.939)$<br>$BF3 = \max(0, TEMPJUNE - 6.120)$ |
| 140W, 65N | $Y = \max(0, 11.289 + 1.091 \times BF8)$<br>$BF2 = \max(0, 62.700 - DCMAY)$<br>$BF8 = \max(0, TEMPAPRI + 10.547) \times BF2$ |
| 142.5W, 65N | $Y = \max(0, -163.527 + 13.843 \times BF1 + 220.481 \times BF3 + 62.554 \times BF4)$<br>$BF1 = \max(0, DCJULY - 337.674)$<br>$BF3 = \max(0, TEMPJUNE - 9.783)$<br>$BF4 = \max(0, 9.783 - TEMPJUNE)$ |
| 145W, 62.5N | $Y = \max(0, 13.861 + 7.114 \times BF1 + 25035.348 \times BF3 - 21217.652 \times BF5)$<br>$BF1 = \max(0, DCJUNE - 167.287)$<br>$BF3 = \max(0, MSRJUNE - 0.004)$<br>$BF5 = \max(0, MSRJUNE - 0.001)$ |
| 145W, 65N | $Y = \max(0, -1231.302 + 314.707 \times BF2 + 81.678 \times BF4 + 8.472 \times BF5 + 64.587 \times BF7 + 95.313 \times BF8 + 74.166 \times BF11)$<br>$BF2 = \max(0, 8.135 - TEMPAUG)$<br>$BF4 = \max(0, 66.700 - DCMAY)$<br>$BF5 = \max(0, DCJULY - 270.303)$<br>$BF7 = \max(0, 36.630 - FFMCJUNE)$<br>$BF8 = \max(0, DMCMAY - 0.084)$<br>$BF11 = \max(0, TEMPAPRI + 10.753)$ |
| 147.5W, 62.5N | $Y = \max(0, 48.363 + 4891.161 \times BF2)$<br>$BF2 = \max(0, MSRAPRIL - 0.021)$ |
| 147.5W, 65N | $Y = \max(0, 36.584 + 52.402 \times BF2)$<br>$BF2 = \max(0, 35.230 - FFMCJUNE)$ |
| 150W, 62.5 | $Y = \max(0, 12.067 + 34.659 \times BF4)$<br>$BF3 = \max(0, 9.465 - TEMPJULY)$<br>$BF4 = \max(0, DMCJUNE - 0.130) \times BF3$ |
| 150W, 65N | $Y = \max(0, -169.078 - 3259.911 \times BF6 + 1192.324 \times BF8 + 2073.436 \times BF10 + 423.590 \times BF13)$<br>$BF6 = \max(0, DMCJULY - 1.181)$<br>$BF8 = \max(0, DMCJULY - 1.974)$<br>$BF10 = \max(0, DMCJULY - 0.658)$<br>$BF13 = \max(0, 1.463 - DMCJUNE)$ |
| 152.5W, 62.5N | $Y = \max(0, 17.677 - 307.055 \times BF2 + 262.489 \times BF4)$<br>$BF1 = \max(0, DMCJUNE - 0.187)$<br>$BF2 = \max(0, DMCMAY - 3.084) \times BF1$<br>$BF4 = \max(0, DMCMAY - 2.432) \times BF1$ |
| 152.5W, 65N | $Y = \max(0, -623.691 + 175.802 \times BF1 + 498.019 \times BF2 + 448.783 \times BF5 + 4.265 \times BF8 - 198.457 \times BF11)$<br>$BF1 = \max(0, TEMPAUG - 9.239)$<br>$BF2 = \max(0, 9.239 - TEMPAUG)$<br>$BF5 = \max(0, TEMPAPRI + 4.583)$<br>$BF8 = \max(0, DCJULY - 214.584)$<br>$BF11 = \max(0, TEMPAPRI + 6.827)$ |
| 155W, 62.5N | $Y = \max(0, -560.543 + 30.780 \times BF2 + 322.213 \times BF3 + 144.693 \times BF6 + 20005.117 \times BF8 - 0.689 \times BF11)$<br>$BF1 = \max(0, DCMAY - 59.242)$<br>$BF2 = \max(0, 59.242 - DCMAY)$<br>$BF3 = \max(0, MSRJULY + 0.106806E\text{-}08) \times BF1$<br>$BF6 = \max(0, TEMPAUG - 6.658)$<br>$BF8 = \max(0, 0.002 - MSRAUG) \times BF1$<br>$BF11 = \max(0, DCJULY - 324.065) \times BF1$ |
| 155W, 65N | $Y = \max(0, 40.693 + 11.303 \times BF1)$<br>$BF1 = \max(0, DCJULY - 354.110)$ |
| 157.5W, 60N | $Y = \max(0, -518.197 + 357.580 \times BF3 + 18523.148 \times BF6 + 226.227 \times BF7 + 78.687 \times BF9)$<br>$BF3 = \max(0, TEMPJUNE - 9.460)$<br>$BF6 = \max(0, 0.026 - MSRAUG)$<br>$BF7 = \max(0, TEMPAUG - 9.855)$<br>$BF9 = \max(0, TEMPMAY - 2.681)$ |
| 157.5W, 62.5N | $Y = \max(0, -979.175 + 15.565 \times BF3 + 15085.198 \times BF4 + 5.638 \times BF5 + 28.716 \times BF7)$<br>$BF3 = \max(0, 74.471 - DCMAY)$<br>$BF4 = \max(0, MSRAPRIL - 0.346190E\text{-}09)$<br>$BF5 = \max(0, DCJULY - 220.374)$<br>$BF7 = \max(0, 48.387 - FFMCJULY)$ |
| 157.5W, 65N | $Y = \max(0, -13.953 + 188.621 \times BF1 + 20.525 \times BF3 + 7.542 \times BF13)$<br>$BF1 = \max(0, TEMPAUG - 11.568)$<br>$BF3 = \max(0, FFMCJULY - 60.616)$<br>$BF13 = \max(0, DCJUNE - 198.307)$ |
| 160W, 60N | $Y = \max(0, 13.621 + 179.362 \times BF1 + 138.743 \times BF3 + 63.530 \times BF5 - 28.852 \times BF18)$<br>$BF1 = \max(0, TEMPJUNE - 9.757)$ |

*Continued*

 

**Table A1.** (*Contd.*)

| Location | Model |
|---|---|
| | BF3 = max(0, TEMPMAY−4.619) |
| | BF5 = max(0, DMCJULY−5.503) |
| | BF18 = max(0, DMCJULY−1.600) |
| 160W, 62.5N | $Y$ = max(0, −41.138 + 252.296 × BF1 + 12.634 × BF3 + 1219.904 × BF10) |
| | BF1 = max(0, TEMPJUNE−11.620) |
| | BF3 = max(0, DCJULY−350.397) |
| | BF10 = max(0, MSRAUG−0.039) |
| 160W, 65N | $Y$ = max(0, 52.236 + 620.239 × BF1 + 56.485 × BF12−28.481 × BF14 + 355.372 × BF16−126.289 × BF18) |
| | BF1 = max(0, MSRJULY−0.299) |
| | BF12 = max(0, DMCJULY−14.877) |
| | BF14 = max(0, DMCJULY−8.271) |
| | BF16 = max(0, TEMPAUG−11.693) |
| | BF18 = max(0, TEMPAUG−10.303) |
| 162.5W, 62.5N | $Y$ = max(0, 4.911−0.112 × BF9 + 8.838 × BF11) |
| | BF1 = max(0, DCAUG−160.252) |
| | BF9 = max(0, 3.719−DMCJULY) × BF1 |
| | BF11 = max(0, 0.033−MSRJULY) × BF1 |